Fall 2013

New sensorless, efficient optimized and stabilized V/f control for PMSM machines

Seyed Hesam Jafari

Department:

NEW SENSORLESS, EFFICIENT OPTIMIZED AND STABILIZED V/F CONTROL FOR PMSM MACHINES

by

SEYED HESAM JAFARI

A THESIS

Presented to the Faculty of the Graduate School of the

MISSOURI UNIVERSITY OF SCIENCE AND TECHNOLOGY

In Partial Fulfillment of the Requirements for the Degree

MASTER OF SCIENCE IN ELECTRICAL ENGINEERING

2013

Approved by

Dr. Jonathan Kimball, Advisor
Dr. Keith Corzine, Co Advisor
Dr. Mehdi Ferdowsi

ABSTRACT

With the rapid advances in power electronics and motor drive technologies in recent decades, permanent magnet synchronous machines (PMSM) have found extensive applications in a variety of industrial systems due to its many desirable features such as high power density, high efficiency, and high torque to current ratio, low noise, and robustness. In low dynamic applications like pumps, fans and compressors where the motor speed is nearly constant, usage of a simple control algorithm that can be implemented with least number of the costly external hardware can be highly desirable for industry.

In recent published works, for low power PMSMs, a new sensorless volts-per-hertz (V/f) controlling method has been proposed which can be used for PMSM drive applications where the motor speed is constant. Moreover, to minimize the cost of motor implementation, the expensive rotor damper winding was eliminated. By removing the damper winding, however, instability problems normally occur inside of the motor which in some cases can be harmful for a PMSM drive. As a result, to address the instability issue, a stabilizing loop was developed and added to the conventional V/f.

By further studying the proposed sensorless stabilized V/f, and calculating power loss, it became known that overall motor efficiency still is needed to be improved and optimized. This thesis suggests a new V/f control method for PMSMs, where both efficiency and stability problems are addressed. Also, although in nearly all recent related research, methods have been applied to low power PMSM, for the first time, in this thesis, the suggested method is implemented for a medium power 15 kW PMSM.

A C2000 F2833x Digital Signal Processor (DSP) is used as controller part for the student custom built PMSM drive, but instead of programming the DSP in Assembly or C, the main control algorithm was developed in a rapid prototype software environment which here Matlab Simulink embedded code library is used.

ACKNOWLEDGMENTS

First and foremost I would like to say thanks to my advisors Dr. Jonathan Kimball and Dr. Keith Corzine for their time, patience, and dedication to my higher learning. I highly appreciate them trusting me and utilizing their vast knowledge of electrical engineering to aid in my advancement of becoming a better researcher and a professional engineer prepared to work in industry.

I should also say thanks to my thesis committee Dr. Mehdi Ferdowsi for the valuable advice he gave to me through these last years. Here, at MST I took nearly all my courses with my thesis committee members where they helped me to increase my knowledge and develop a solid background in the area of power electronic, electrical vehicle and motor drive.

This work was supported by the Department of Energy under contract DE-EE0002012.

Next, I would like to thank God that gave me enough power to write this thesis and then my parents for their support and direction through my journey of this master's program. I owe them all of my life successes and accomplishments and always thankful to them because they sacrificed their life for me and my sister.

TABLE OF CONTENTS

LIST OF ILLUSTRATIONS

Page

LIST OF TABLES

Page

NOMENCLATURE

Symbol	Description
l	Length of the Conductor
F	Exerted Force
B	Magnetic Field
ϕ_0	Power Factor Angle
I_s	Magnitude of the Current
E_s	Magnitude of the Voltage Vector
r_s	Stator Winding Resistance
λ_m	Rotor Permanent-Magnet Flux
f_o	Applied frequency
ω_e	Electrical Speed
B_m	Viscous Friction Coefficient
V_s	Stator Voltage Magnitude
J	Inertia of the Motor and the Load System
V_{rated}	Rated Voltage Phase to Phase
T_{lrated}	Load Torque
n	Number of Poles of the Motor
i^r_{qs}	Rotor q Axes Current
i^r_{ds}	Rotor d Axes Current
L	Motor Inductance
v_{dc}	DC Power Supply
d	Modulation Index
CAN	Communication Area Network
PMSM	Permanent Magnet Synchronized Motor
ADC	Analog to Digital Converter
DSP	Digital Signal Processor

1. INTRODUCTION

1.1. MOTIVATION

When PMSM drives are used for applications like pumps and fans, where high dynamic performance is not a demand, a simple control strategy can be used instead of the sensorless field-oriented- control approach that is heavily dependent on the rotor position sensor. Furthermore, the PMSM damper windings in the rotor assure the synchronization of motion of the rotor with the stator applied frequency, which is the fundamental requirement for synchronous machine control. This allows a stable control of this type of PMSM in an open-loop manner. However, due to the high manufacturing cost and the difficulty to design rotors with damper windings for some type of PMSMs the PMSMs are not generally available with damper windings in the rotor. The PMSMs without damper windings in the rotor do not assure the synchronization of motion of the rotor with stator applied frequency under the open-loop control approach. This causes instability problems in those PMSMs under the open-loop control approach and an additional signal is required to the controller in order to assure the synchronization and the stable operation. Moreover, a PMSM using a damper winding may not have stability issue but its functionality and operations may not be efficient and acceptable. Further study shows that only i_q stator current can contribute in effective torque generation while i_d stator current can increase the overall motor loss therefore the efficiency issue needs to be addressed for any PMSM.

1.2. PERMANENT MAGNET SYNCHRONOUS MACHINES (PMSM)

The permanent-magnet synchronous machine (PMSM) drive has emerged as a top competitor for a full range of motion control applications [1, 2, 3]. For example, the PMSM is widely used in machine tools, robotics, actuators, and is being considered in high-power applications such as vehicular propulsion and industrial drives. It is also becoming viable for commercial/residential applications. The PMSM is known for having high efficiency, low torque ripple, superior dynamic performance, and high power density.

These drives often are the best choice for high-performance applications and are expected to see expanded use as manufacturing costs decrease. The PMSM is a synchronous machine in the sense that it has a multiphase stator and the stator electrical frequency is directly proportional to the rotor speed in the steady state. However, it differs from a traditional synchronous machine in that it has permanent magnets in place of the field winding and otherwise has no rotor conductors. The use of permanent magnets in the rotor facilitates efficiency, eliminates the need for slip rings, and eliminates the electrical rotor dynamics that complicate control (particularly vector control). The permanent magnets have the drawback of adding significant capital cost to the drive, although the long term cost can be less through improved efficiency. The PMSM also has the drawback of requiring rotor position feedback by either direct means or by a suitable estimation system. Since many other high performance drives utilize position feedback, this is not necessarily a disadvantage. A conceptual drive system is pictured in Figure 1.1. There, a speed, position, or torque command is input to the drive system. The motion controller implements feedback control based on mechanical sensors (or estimators). The controller generates commands for the electrical variables to obey. The electrical control block converts its input commands into commands for the power converter/modulator block and sometimes utilizes feedback of voltage or current. The power converter block imposes the desired electrical signals onto the PMSM machine with the connected load.

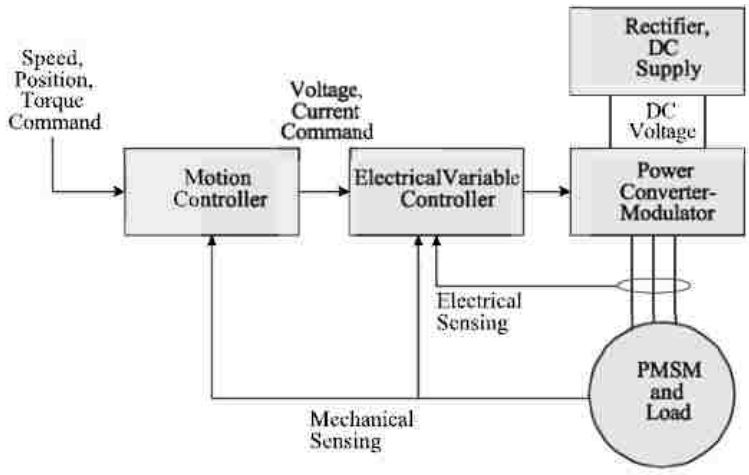

Figure 1.1. Diagram of conceptual drive system

As in all electrical motors, a PMSM has two principle parts, a moving part and a stationary part which are called rotor and stator. The phase windings are found in the stator and can be configured in different ways, for example as sinusoidal, trapezoidal or the more common concentrated winding. There are usually three phase windings since most PMSMs are three phase motors, thus each winding is excited by a different phase. When a current runs through windings a force is exerted on the current due to the magnetic field of the rotor. This phenomena is called the Lorentz force and is described by equation

$$F = \vec{l} \cdot (\vec{I} \times \vec{B}) \tag{1}$$

Here *F* is the force exerted, l is length of the conductor, I is the current flowing in the conductor and B is the external magnetic field present. The counter force to equation (1) is that causes the rotation of the rotor and transform electrical energy to mechanical energy.

In Figure 1.2 the cross section of a simplified PMSM with concentrated winding is depicted. The three phase windings are presented by u, v, w respectively and the rotor is modeled as a simple magnet bar, thus this motor has two poles. The max torque generation can achieved when the current and the magnetic vectors field are orthogonal. Therefore, the goal of any motor control algorithm should be to keep the current flowing in the stator winding orthogonal to the magnetic field of the rotor.

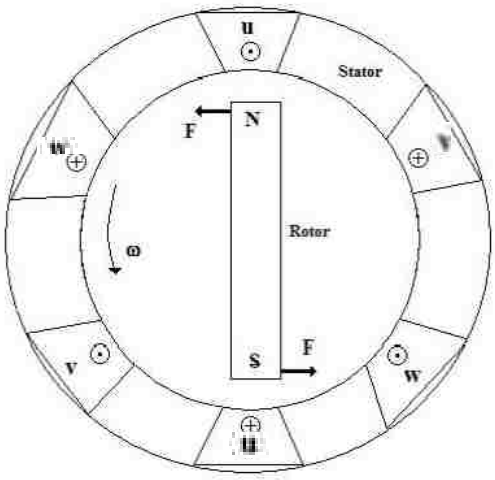

Figure 1.2. Two poles salient PMSM

2. CONTROL METHOD

2.1. REVIEW OF THE SENSORLESS CONTROLLING METHOD OF PMSM

With the rapid advances in power electronics and motor drive technologies in recent decades, permanent magnet synchronous machines (PMSM) have found extensive applications in a variety of industrial systems due to their many desirable features such as high power density, high efficiency, and high torque to current ratio, low noise, and robustness. However, using a PMSM also is associated with some limitations. One major drawback of the most commonly used PMSM drive systems is that the control algorithm requires the knowledge of the rotor position or speed, which requires the usage of an encoder or a resolver, increasing the final machine cost and decreasing system reliability. The use of these rotational transducers escalates the complexity of the motor construction, complicates the production process, and increases the final machine cost, while at the same time decreases system reliability. Sensorless control for PMSM has been a desired field of study of researchers in recent years, and a large number of sensorless control methods have been proposed over the years [4, 5, 6, 7, 8, 9, 10]. Among those methods, some utilize the position dependence of the back electromotive force (EMF), some rely on rotor saliency characteristics, and the injection of various kinds of test signals is used in some of recent papers. In [9], the authors proposed a novel modified back EMF observer for rotor speed estimation based on sliding mode observer theory using Lyapunov stability criteria. In [10], the sensorless operation of PMSM was extended to all four quadrants and at significantly low speed, by measuring the current derivative during the zero voltage switching vectors. The majorities of those methods are based on the involved algorithms, and are proposed for the high dynamic application. However, for applications where high dynamic performance is not a demand, such as pump and fan motor drive systems, an inexpensive, a simpler and more robust method is often desired. Moreover, due to the high manufacturing cost and difficulty to design rotor with damper winding for some type of PMSMs, the PMSMs are not generally available with damper winding on the rotor. As a result, using the open-loop V/f control approach causes some instability problems in the PMSM performance. In [11], Perera et al. address the inherent instability issue associated with the open-loop V/f control for PMSM that do

not have damper windings in the rotor, and then proposed such a sensorless control technique that was integrated into a V/f control method in order to resolve the mentioned problem. By modulating the applied voltage frequency proportional to the perturbations in the input power, the method achieved a stable control in a wide frequency range while maintaining a constant stator flux linkage of the motor.

Further detailed study of the method proposed by Perera et al. revealed that although the suggested stabilized sensorless control is very effective, the overall PMSM drive control is not optimized. Especially, in certain operating conditions, the non-optimal choice of the stator flux linkage can lead to low motor efficiency. In this thesis, an efficiency improvement method is proposed that can be combined with the sensorless stable control in [11] to attain efficient V/f operation of PMSM. The proposed method is easy to implement and does not require any additional hardware changes or measurement signals.

2.2. VOLTAGE CONTROL METHOD AND STABILITY ANALYSIS

In the proposed V/f control method, the magnitude of the voltage is calculated in order to keep a stator flux linkage constant in the PMSM. With a constant stator flux linkage, the PMSM has the same torque-producing capability in all operating frequency ranges. The steady-state vector diagram of the PMSM is shown in Figure. 2.1 can be used to explain the calculation of the voltage magnitude.

In the triangle *OAB* shown in Figure 2.1, *AC* is drawn perpendicular to *OB*. From the *OAB* triangle the steady-state magnitude of the voltage vector can be obtained as

$$V_s = \mathrm{BC} + \mathrm{CO} = \mathrm{I_s r_s cos\phi_0} + \sqrt{\mathrm{E_s^2} - \mathrm{I_s^2 r_s^2 \sin^2 \phi_0}} \quad (2)$$

Where I_s is the magnitude of the current and the vector E_s is the magnitude of the voltage vector induced by stator flux linkage, and ϕ_0 is the power factor angle, the phase difference between current and voltage ; all are in steady state. r_s is the stator winding resistance per phase. Using trigonometric relationship, we can simplify the above mathematical equation like

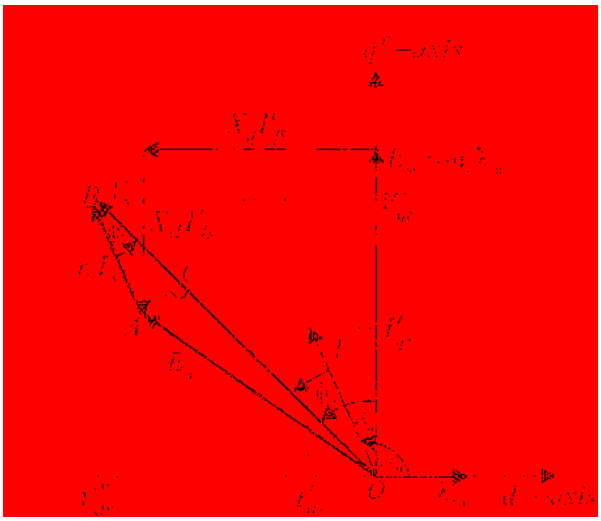

Figure 2.1. Steady-state vector diagram of the PMSM in synchronized reference frame

$$V_s = I_s r_s \cos\phi_0 + \sqrt{E_s^2 + I_s^2 r_s^2 \cos^2\phi_0 - I_s^2 r_s^2} \tag{3}$$

The stator-flux-induced Voltage E_s in previous equation can be calculated from the required steady-state constant stator flux. The constant magnitude of the stator flux vector is selected as the rotor permanent-magnet flux λ_m. With this selection of the magnitude of the stator flux, can be calculated from:

$$E_s = 2\,\pi\, f_0 \lambda_m \tag{4}$$

In above equation, f_o is the frequency applied to the machine. Furthermore, the term $I_s \cos\varphi$ in (3) is the stator current component along with the stator voltage vector. By transforming the measured phase currents to the stator voltage fixed reference frame this term can instantaneously be calculated as

$$i_s cos\phi = \frac{2}{3}\left[i_{as} cos\theta_e + i_{bs}\, cos\left(\theta_e - \frac{2\pi}{3}\right) - (i_{as} + i_{bs})\, cos\left(\theta_e + \frac{2\pi}{3}\right)\right] \tag{5}$$

Where i_s and ϕ are the instantaneous values of the magnitude of the current vector and the power-factor angle, respectively. Moreover, i_{as} and i_{bs} are the measured phase currents and θ_e is the position of the voltage vector in the stationary reference frame.

From the vector diagram shown in Figure 2.1, someone can easily find the magnitude of i_{ds} &i_{qs}, but since the stator currents are measured by current sensorless it is somehow more desirable to express the magnitude of stator current base on i_{as} & i_{bs} . To fulfill this requirement, we can apply the Clarke transformation where we have following equations:

$$\mathrm{i_{ds}} = \frac{1}{3}(\mathrm{i_{as}} + 2\mathrm{i_{bs}})^2 \qquad \mathrm{i_{qs}} = \mathrm{i_{bs}} \tag{6}$$

By using the equation (5), final simple form of the equation the absolute value of the stator current base on the a-b component can be found from equation (6)

$$i_s = \sqrt{(I_{ds}^s)^2 + \left(I_{qs}^s\right)^2} = \sqrt{\frac{1}{3}(i_{as} + 2i_{bs})^2 + (i_{as})^2} \tag{7}$$

Using the instantaneously calculated values and the commanded value for the $\mathrm{E_s}$ the final expression for calculation of magnitude of the voltage command $v^*{}_s$ can be written as

$$\mathrm{V_s} = \mathrm{I_s r_s}\cos\phi_0 + \sqrt{(2\pi \mathrm{f_o}\lambda_\mathrm{m})^2 + \mathrm{I_s^2 r_s^2}\cos^2\phi_0 - \mathrm{I_s^2 r_s^2}} \tag{8}$$

The real implementation of equation (7) is shown in Figure 2.2 in the block diagram format. Low Pass Filters (LPF) are used to remove the high frequency ripple associated with calculated currents i_s and $i_s \cos\phi$. Moreover, f_0 is the electrical speed applied to PSMM stator which is directly proportion with commanded speed. In V/f

controlling method the ratio of the applied stator voltage and frequency is fixed and constant.

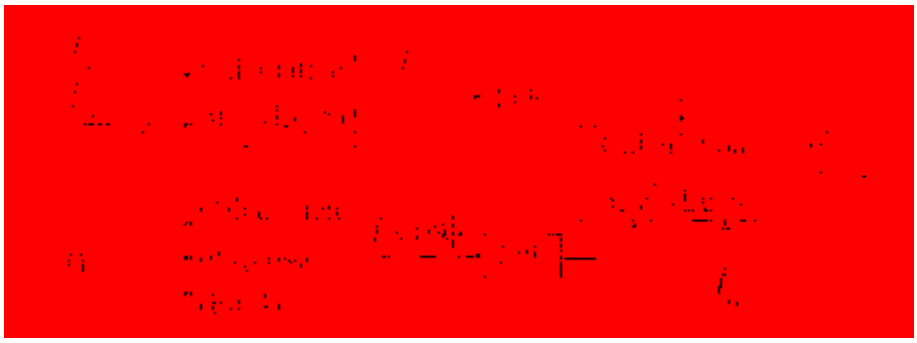

Figure 2.2. Calculation of the voltage command

The preliminary drive configuration with the above-discussed voltage control method is shown in Figure 2.3.

2.3. STABILITY ANALYSIS

One of the most important aspect of PMSM drive performance is its dynamic response which means that whether it can exhibit a smooth and stable response to different inputs at many various conditions which the PMSM may encounter in practice.

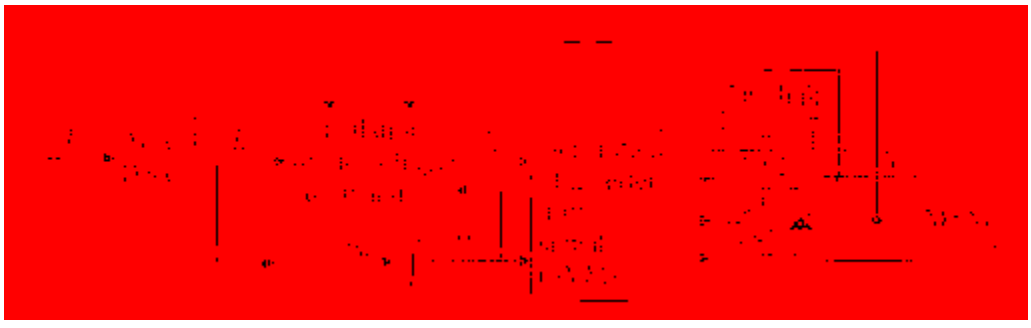

Figure 2.3. Primary drive configuration with V/f control method

As an example, in this case, it must be verified in the case when the frequency of applied voltage and current get changed, the output of system such as rotor speed should

gradually reach to the final value very smoothly although before reaching to this point it may exhibit a negligible oscillatory behavior. In this part, stability analysis is going to be performed for PMSM motor which does not have damper winding. To analyze the stability of the PMSM under constant stator flux linkage control, the linearized PMSM model is used. The eigenvalues of the state transition matrix of the linearized PMSM model will reveal the stability behavior of the PMSM for all scenarios. Using the linearized form of the equation accurate for PMSM, we will have the following equations:

$$pi_{qs} = \frac{-i_{qs}}{\sigma\tau_s} - \frac{\omega_r}{\sigma}\left(\frac{\lambda_m}{L_d} + i_{ds}\right) + \frac{v_s \cos(\delta)}{\sigma L_d} \qquad (9)$$

$$pi_{ds} = \frac{-i_{ds}}{\tau_s} - \left(\sigma\omega_r i_{qs}\right) - \frac{v_s \sin(\delta)}{L_d} \qquad (10)$$

$$p\omega_r = \frac{3}{2J}\left(\frac{n}{2}\right)^2 \left[\lambda_m i_{qs} + L_d(1-\sigma) i_{qs} i_{ds}\right] - \frac{1}{J} B_m \omega_r - \frac{n}{2J} T_l \qquad (11)$$

In (8) - (11):

$$\tau_s = L_{d/r_s} \quad , \qquad \sigma = \frac{L_q}{L_d} \qquad (12)$$

The machine linear state equations (8)–(12) have the state form

$$\dot{x} = f(x, u) \qquad (13)$$

where is the vector of the machine state variables and is the nonlinear function of the state and the inputs . The linearized system equations of this nonlinear system have the form

$$\dot{\Delta x} = A(x)\Delta x + B(x)\Delta u \qquad (14)$$

in which Δx is the perturbations matrix for state variables, A(x) is the state transition matrix, Δu is the input perturbation matrix, and B(x) is the input matrix, finally, The obtained linearized PMSM model can be written as in the matrix equation (13), moreover, When deriving this model, it is considered that the input voltage and the frequency to the PMSM are constant steady state values, i.e., perturbations $\Delta v_s=0$ and $\Delta\omega_e=0$.

Using equation (13) which its derivation process is explained in [11] , some inherent characteristic of the system such as stability issue can be studied from equation (15).

The state transition matrix in (15) can be solved by using machine parameters and the steady-state value of the machine variables (voltage, current, etc.) presented in table 2.1. In this thesis, machine parameters are chosen from [11], which are:

$$p\begin{bmatrix}\Delta i_{qs}^r\\ \Delta i_{ds}^r\\ \Delta\omega_r\\ \Delta\delta\end{bmatrix} = \begin{bmatrix} -\frac{1}{\sigma\tau_s} & -\frac{\omega_0}{\sigma} & -\frac{1}{\sigma}\left(\frac{\lambda_m}{L_d}+I_{ds}^r\right) & -\frac{V_s}{\sigma L_d}\sin(\delta_0)\\ \sigma\omega_0 & -\frac{1}{\tau_s} & \sigma I_{qs}^r & -\frac{V_s}{L_d}\cos(\delta_0)\\ \frac{3}{2}\frac{\left(\frac{n}{2}\right)^2}{J}\left[\lambda_m+L_d(1-\sigma)I_{ds}^r\right] & \frac{3}{2}\frac{\left(\frac{n}{2}\right)^2}{J}L_d(1-\sigma)I_{qs}^r & -\frac{B_m}{J} & 0\\ 0 & 0 & -1 & 0\end{bmatrix}\begin{bmatrix}\Delta i_{qs}^r\\ \Delta i_{ds}^r\\ \Delta\omega_r\\ \Delta\delta\end{bmatrix}$$

Table 2.1. PMSM motor parameters which its loci plot is shown in Figure 1.6

$P_{rated} = 2.2\ kW$	$V_{rated} = 380\ V$	$\lambda_m = .48\ V.s.rad^{-1}$
$T_{lrated} = 12$ N. m	$r_s = 3.3\Omega$	$Poles = 6$
$L_q = 57.09\ mH$	$L_d = 41.59\ mH$	$B_m = 20.44 * 10^{-4} N.m.s.rad^{-1}$
$J = 10.07 * 10^{-3} kg.m^2$		$\omega_{rated} = 1750 \frac{r}{min}$

The paper also plots the calculated eigenvalues of the state transition matrix of A(X) in (15), under no load, i.e., $v_s = E_m$ (back electromotive force (EMF) produced by rotor permanent magnets), as a function of the applied frequency. Figure 2.4 shows Loci of the rotor poles under different load conditions. From below figure, the system goes unstable when the electrical frequency greater than 15 Hz which means that if rotor speed start increasing once time it pass this frequency the motor become unstable and its speed get back to the zero)

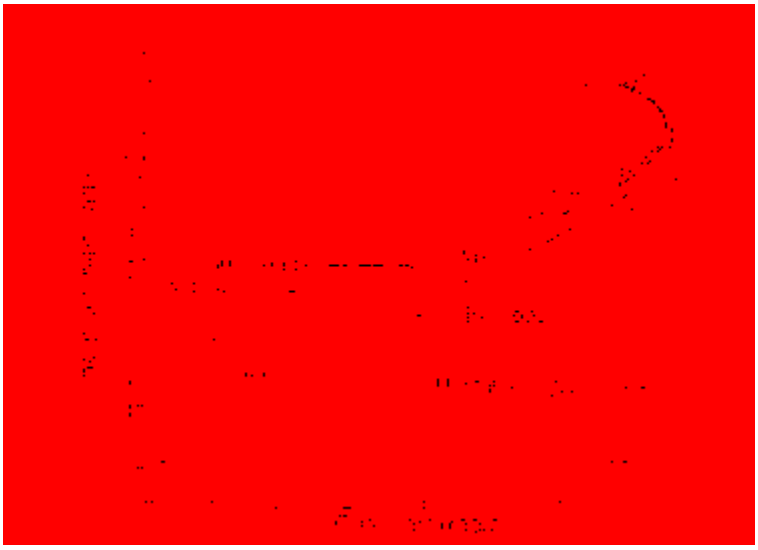

Figure 2.4. Loci of the rotor poles under different load conditions, as a function of the applied frequency

2.4. FREQUENCY MODULATION TECHNIQUE

The PMSM's instability behavior after exceeding a certain applied frequency observed in previous section is due to the nonexistence of rotor circuits (i.e., damper windings) and, therefore, the weak coupling between electrical and mechanical modes of the machine. The stator and rotor poles move away from each other and, after exceeding a certain applied frequency, the poles of the system cross over to the instability region of the **s** plane (right side of imaginary axis), having a small positive real part. Improvement of instability issue can be achieved by a proper modulation of the applied frequency of the machine.

The system becomes unstable during transient state where the motor tries to follow an increase in speed. If the control system employed for PMSM drive just relies on the open loop V/f method, the electrical speed and frequency are predefined and they increase linearly without considering the transient and instantaneous condition PMSM may face (there is not any simultaneous adjustment, and no flexibility), and in many cases the real PMSM is not able to follow the predefined function which leads the system toward instability condition. However, if the commanded electrical speed being able to adjust itself base on its internal parameters perturbation, a stable behavior can be seen from the system, the key parameter having dramatic changes during transient mode is input power disturbance, and due to the fact that this parameter has direct relation with rotor speed, stabilization loop can be implemented base on the idea of changing commanded speed base on the input real power distribution. Therefore, ω_e is a new variable added into the old A(x) matrix meaning that by choosing the appropriate parameters a new transfer function can be derived. To find a new state space where electrical speed is one its state, using input real power can be a good starting point. As a matter of the fact, the applied frequency should be modulated as:

$$\Delta\omega_e = -k_p \Delta p_e \tag{16}$$

In the simulation, K_p = 2.4 is used. Δp_e is the AC component of real input power which must be filter out from DC value. Therefore, a HPF which has small cut off frequency can be implemented to extract the AC component. Δp_e can be written as

$$\Delta p_e = \frac{s}{s+\frac{1}{\tau_h}} P_e \quad (17)$$

$$P_e = \frac{3}{2} V_s [i^r_{qs} \cos\delta - i^r_{ds} \sin\delta] \quad (18)$$

Where τ_h is the high-pass filter time constant, and in this simulation its value should be τ_h= .064. Substituting Δp_e from (17) in (16), and using equation (18) which present real input power for a salient pole PMSM, the new state transition matrix can be calculated which is fully described given in [11], and using the eigenvalues of new state space matrix, it is easily possible to study the effectiveness of the stabilizing loop, which modulates the applied frequency of the system. Figure 2.5 shows the rotor poles of the system, which are obtained from the new $A'(x)$, under different load conditions as a function of the applied frequency.

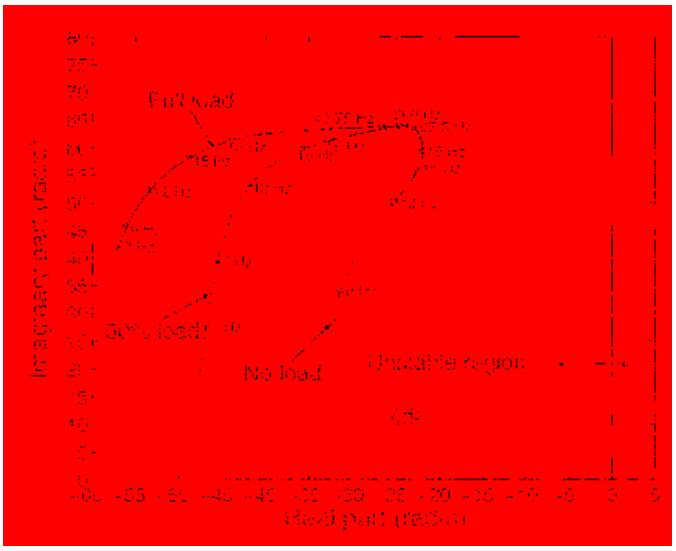

Figure 2.5. Measured rotor speeds at different frequencies, under no load

Comparing Figures. 1.6 and 1.7 helps readers sense easily the effectiveness of the stabilizing loop in the system, and it is obvious that adding stabilized loop which modulate the input frequency of the input parameters of the motor can improve the motor performance, and solve stability issue. Finally, Figure 2.6 show the block diagram of stability loop.

The stability analysis described here is carried out for a salient PMSM which is a general case. Therefore, performing the same procedures for round rotor PMSM, the same results can be found.

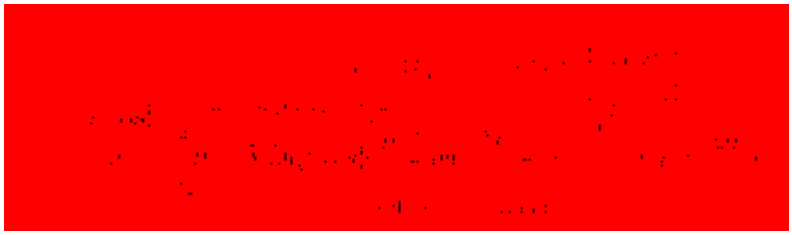

Figure 2.6. Derivation of the frequency modulation signal Δw_e

2.5. EFFICIENCY OPTIMIZATION OF THE STABILIZED V/F CONTROL

In the previous section, it was shown that even with large load torque sudden changes, the control was capable of maintaining stable operation in a wide frequency range. However, further study indicated that the control is not optimized in terms of overall system efficiency. The goal of this part is to improve the efficiency of the system without sacrificing its stability features. Considering a round rotor PMSM, the torque equation can be found from

$$T_e = \frac{3P}{2} \lambda'_m i_q \tag{19}$$

From the above equation, it can be seen that only *q*-axis current contribute in torque production, and any *d*-axis current component only contributes to machine losses. As a result, to improve the efficiency by keeping the d-axis current component close to zero, nearly all of the currents absorbs by the PMSM have contribution in torque production. The vector diagram of a PMSM in such an operating mode is shown in Figure 2.7. From the vector diagram in Figure 2.7, it can be seen that if the *d*-axis current i_d is zero, the current vector I_s is aligned with $\omega_r \lambda_m^{'}$. The reactive power also can be calculated from equation (20).

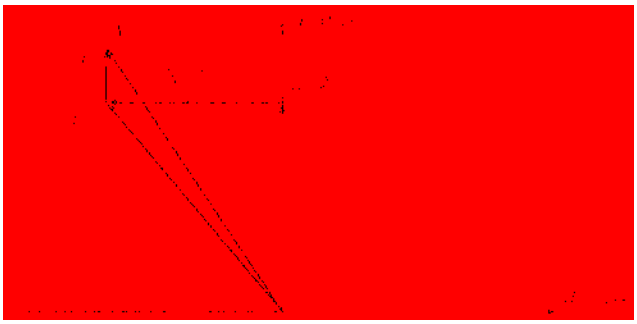

Figure 2.7. Vector diagram of PMSM with maximum torque per amp

$$Q_{in} = \frac{3}{2}\left(V_{qs} i_{qs}\right) = \frac{3}{2}\left(V_s i_{qs}\right) \qquad (20)$$

Thus the current vector can be aligned with the back EMF vector by keeping the reactive power drawn by the PMSM at zero. Since the reactive power in the electrical machines are controlled by adjusting the magnitude of the stator voltage magnitude, a proportional-integral (PI) controller can be used to generate the adjustment Δv_s^* from input reactive power which was found in equation (20).

Finally, Figure 2.8 shows the complete diagram of the proposed efficiency-optimizing method for V/f control, coupled with the stabilization loop we have designed in earlier parts of this report.

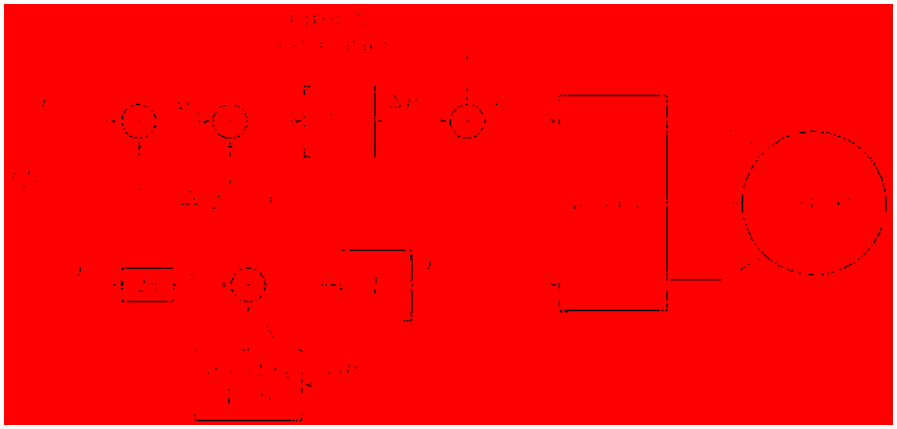

Figure 2.8. Final control diagram for PMSM after adding the stabilized and efficiency loop to the preliminary configuration

3. DSP IMPLEMENTATION USING MATLAB/SIMULINK

3.1. INTRODUCTION

In the present day, time efficiency and flexibility are getting considered highly important in research and product development throughout all industry fields. It also applies to the development, implementation and testing of control algorithms for the electrical motors. The rapid development in computer technology, computer science and electronic during last decades allow electrical engineers and field researchers to easily bring new, complex and efficient motors control algorithms into the practice which now days mainly are implemented on microprocessors. As a result, it has led to a more energy efficient use of electrical motors. Something that can help to the vast energy savings in industrialized countries in which 30% to 40% of the electrical energy consumption is due to the usage of electrical motors.

The process of programming a microprocessor and microcontroller for real time applications is a tedious and time consuming task which must be done with aid of some computer languages like C or Assembly. Furthermore, due to the lack of computer programming skill, many power electrical engineers have difficulties with implementation of a new efficient controlling method for a particular electrical machine. However, during last decade a new approach for microcontroller programming has been developed which is denoted Computer Automated Control System Design (CACSD) and it mainly put emphasis on that embedded system programming should be performed in a graphical environment and thus intuitive. As a matter of fact, in this new scheme, any algorithms are implemented using graphical blocks containing invisible C or Assembly codes and out of this, scheme code is auto generated by the CACSD program environment. In general, this approach is a lot faster than writing the code by hand, something allows developers to spend more time on improving the performance of their programs instead of wasting the time to write and debug their C code errors.

The purpose of this chapter is to examine a rapid prototyping approach using a CACSD to develop and implement a new motor control algorithm on a Digital Signal Processor (DSP), but instead of programming the DSP in Assembly or C, the main control algorithm will be performed in the Matlab/Simulink environment which is

developed by MathWorks^{TM}. The control algorithm is implemented as block scheme in Simulink, and out of this Simulink, Matlab can auto generate C-code needed to program an embedded target like a DSP. Moreover, we also need to use Real-Time Workshop (RTW) Embedded Coder to program our DSP.

It is worthy to mention here that the prime objective of this project is not to develop a very efficient implementation in terms of motor step response and speed reference tracking, but rather to develop a real time test platform that is easy to understand and to evaluate the Mathworks CACSD environment from a user perspective.

The stabilized and efficient sensorless V/f method was implemented on a system which Matlab & Simulink 2012b was installed on it. The additional packages required for target specific code generation for the TI C2000 family are; Real Time Workshop v8.0, Real Time Workshop Embedded Coder v5.0, Link to code composer v4.1 and Target for TI C2000. In addition to the Matlab software, in order to program DSP, Code Composer Studio v4 is needed to load generated C-code on the DSP.

An implementation of stabilized and efficient sensorless V/f in Matlab/Simulink adapted for code generation with RTW can easily result in a model which is difficult to follow its details. Therefore the model developed in the following sections is divided into several subsystems, where each one is explained individually to make overall model more intuitive and easy to follow.

3.2. TOP LEVEL

The overall DSP program for a stabilized and efficient sensorless V/f is shown in Figure 3.1. The target preference block, here it is F28335 which is shown in grey color block, specifies the setting of the processor. As a matter of the fact, this block tells EC what sort of DSP is being programmed so that it initializes the right peripherals, uses the correct operation frequency, knows how much memory is available, etc. It is important to note that the placement of this block is important. When it is placed on the main screen, everything in the simulation file will be built and compiled. However, if it be used inside of a subsystem block, only that subsystem block will be built and compiled.

Figure 3.2 shows inside of eZdsp unit where user can chose his desired microcontroller from wide range of different microcontrollers supporting rapid

prototyping of Matlab/ Simulink. It is also highly important to choose a proper CPU clock which eventually has effect on the PWM switching frequency and ADC sampling time. As a traditional method of C code programming of DSP in the code composer, we normally import some predefined programs and some math libraries like DSP2833x_PieCtril.c and DSP2833x_SysCtril.c and DSP2833x_Interrupt.c, mainly written and developed by Texas Instrument and control default settings for different peripheral units in a DSP, need to be load on DSP alongside of user main C program. Finally, the Peripherals panel can be seen in Figure 3.2, is one of the most valuable features of rapid prototyping which allow users to easily control such important variables like defining eCAN bitrate and setting up I2C graphically through this panel. For more information please refer to [12].

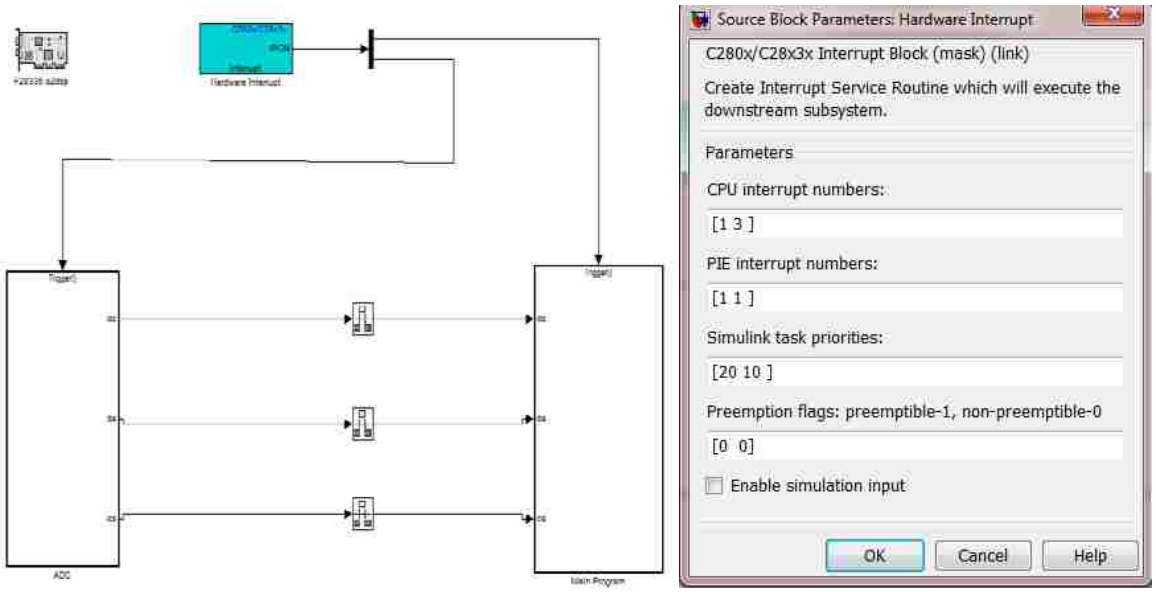

Figure 3.1. The top level in the implementation of DSP program in the Matlab/Simulink, left window, and the properties of the Hardware Interrupt block, right window

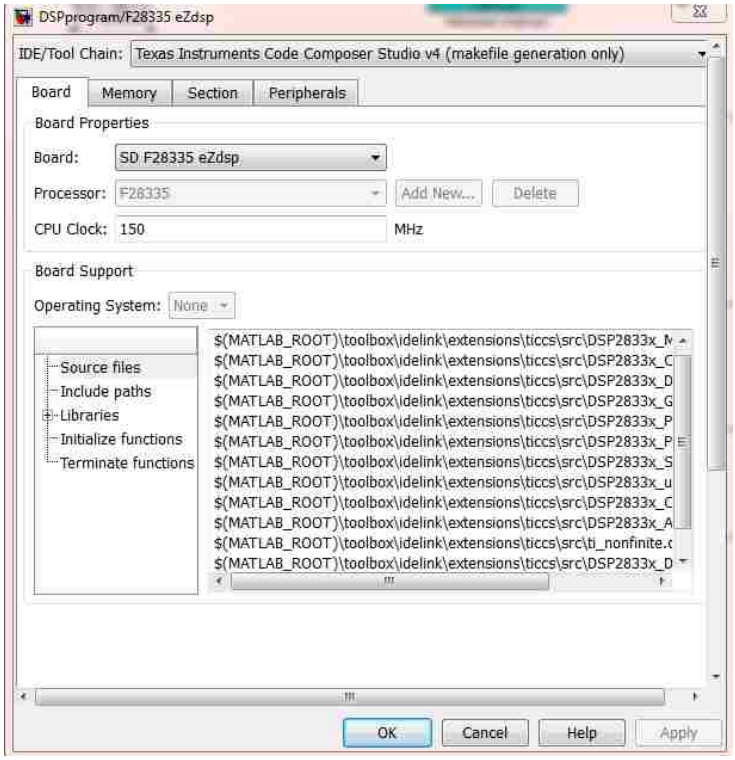

Figure 3.2. Target Preferences block can be fine in Simulink Library Embedded Coder>> Embed Targets

The block should also make a number of changes to the configuration parameters, so the user should always double-check and make sure the parameters are correct. By opening the configuration parameters, which is shown in Figure 3.3, from simulation tab in Simulink, we can have access to broad hardware and software settings. But as simple checking, user needs to ensure that the solver is set to Fixed-step and discrete, the fixed-step size should remain auto. The hardware implementation page should show Texas Instruments, C2000, and Little Endian. By expanding the code generation tree and making sure that the system target file is “idelink_ert.tlc” on the code generation page. Finally, the user needs to open the IDE Link page and select “Build” for the build action option.

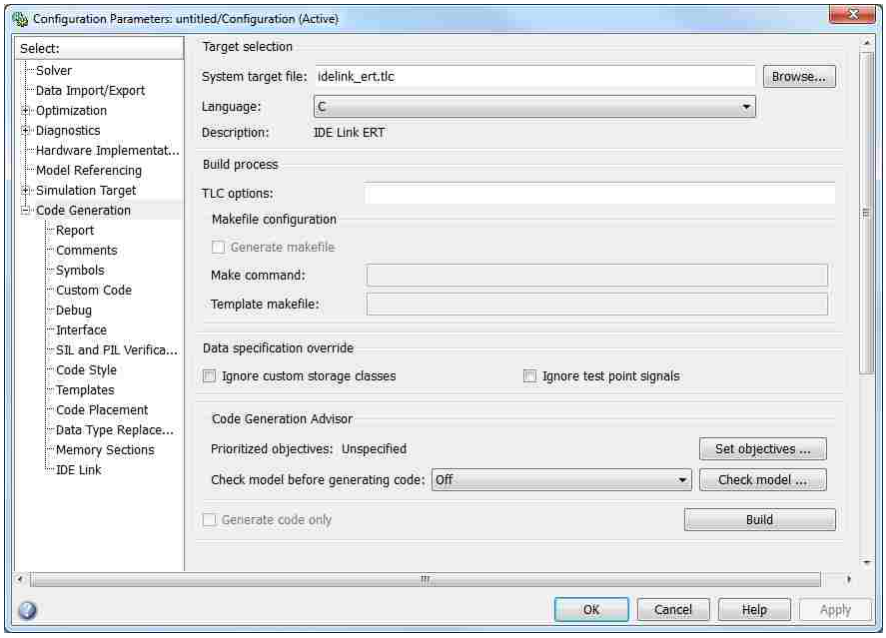

Figure 3.3. Configuration Parameters (simulation tab in Simulink)

For the application where code efficiency has a high priority for the designer, there are a couple of other things that can be done to improve the code output. For one we can set objectives for the generated output code, such as execution efficiency, ROM efficiency, and RAM efficiency.

In Figure 3.1, there are two function call subsystems in the scheme, the right side one which is the main program is the part of the program in which the stabilized and efficient sensorless V/f algorithm is implemented. The next block on the left side is ADC, which is responsible to collect sample current data through the current sensors which are located inside of the PMSM drive. ADC unit do scale and prepare current information for the main program block. From Figure 2.1, someone can also easily find out that subsystems are hooked up to the Hardware Interrupt block which it process interrupt request issued by subsystems in the DSP program and will send trigger signals for subsystem. In the Hardware interrupt block, see again Figure 3.1, the designer can set the Interrupt Service Routine (ISR's) that are to be used in the program and how these shall be prioritized. The ISR generated by the Hardware Interrupt block are connected to the Main program and ADC units which are triggered to be executed asynchronously once its

interrupt is thrown. Since subsystems in our program are executed asynchronously all blocks placed inside of them must have their sample time set to -1, which implies that the sample time is inherited.

The right part of Figure 3.1 shows the properties pane of the Hardware Interrupt Block. To generate an ISR the designer should choose the four parameters, specified on row one to four, that are used by Matlab to describe an interrupt. The first two parameters are the CPU and PIE interrupt numbers, found on row one and two separately. These numbers correspond to a position in the F28335 interrupt table which is shown in Figure 3.4.

In right window of Figure 3.1, two ISR are initialized, here presented in coordinated form (CPU number, PIE number). The first interrupt has coordinates (1, 1), which corresponds to an event coming from the ADC module. Interrupt number two has coordinates (3, 1) which correspond to an event coming from the first ePWM module and it triggers the execution of the Main Program subsystem. Moreover, on the third row the Simulink task priority is set, a low value correspond to a high priority. Here the Main Program subsystem has a higher priority since it is the main task and thus forms the base rate of the model. Figure 3.4 shows F2833x PIE interrupt assignment table which specify related peripheral units interrupt numbers, for more information about interrupt unit inside of the C2000 F2833x please see [13]. The reader should also be aware that process of setting the interrupt units is not yet over because what have been discussed up to this point are related to top level part of a DSP program. To set up the interrupt request, we shall go into subsystem under layer where major DSP peripheral units like ADC, ePWM and CAN are located.

Finally, on the top level page, it can be seen that there are rate transition blocks connected between output and input of ADC and Main Program subsystems. This is a requirement for all signal paths between blocks running on different sample rates. The rate transition block improves the data integrity in the system.

F2833x PIE Interrupt Assignment Table

	INTx.8	INTx.7	INTx.6	INTx.5	INTx.4	INTx.3	INTx.2	INTx.1
INT1	WAKEINT	TINT0	ADCINT	XINT2	XINT1		SEQ2INT	SEQ1INT
INT2			EPWM6_TZINT	EPWM5_TZINT	EPWM4_TZINT	EPWM3_TZINT	EPWM2_TZINT	EPWM1_TZINT
INT3			EPWM6_INT	EPWM5_INT	EPWM4_INT	EPWM3_INT	EPWM2_INT	EPWM1_INT
INT4			ECAP6_INT	ECAP5_INT	ECAP4_INT	ECAP3_INT	ECAP2_INT	ECAP1_INT
INT5							EQEP2_INT	EQEP1_INT
INT6			MXINTA	MRINTA	MXINTB	MRINTB	SPITXINTA	SPIRXINTA
INT7			DINTCH6	DINTCH5	DINTCH4	DINTCH3	DINTCH2	DINTCH1
INT8			SCITXINTC	SCIRXINTC			I2CINT2A	I2CINT1A
INT9	ECAN1_INTB	ECAN0_INTB	ECAN1_INTA	ECAN0_INTA	SCITXINTB	SCIRXINTB	SCITXINTA	SCIRXINTA
INT10								
INT11								
INT12	LUF	LVF		XINT7	XINT6	XINT5	XINT4	XINT3

Figure 3.4. Interrupt vector table

3.3. ADC UNIT AND SUBSYSTEM

Figure 3.5 depict inside of ADC subsystem. As it was mentioned in the previous part, C280/C2833x ADC peripheral block inside of ADC unit first start reading the current signals, and then scale them up to their actual current magnitude and as last and most important step filter out undesirable noises associate with current signals. To do noise cancelation, a LPF with 5 Hz cut off frequency is employed. However, even using this low pas filter; we still observe a major noise component on current signal. Therefore, to better address and alleviate undesirable noise effect, a series of unit delay blocks are employed at the output side of LPF. Figure 3.6 clearly shows how these block is implemented using some delay units. As a matter of the fact, using delay units, which their delay time is defined by trigger unit. Having access to about 25 sample points make it possible to find the sum and then calculate the average value. Therefore, after using these noise cancelation strategies what we expect to see at the output of the ADC subsystem is pure sinusoidal waveforms with very small proportion of noise.

On Figure 3.7, properties panel of the ADC module is shown. C280/C2833x ADC consist from two independent ADC channels A/B which have their own control time base and they are capable to operate in Simultaneous mode and sequence mode. By selecting

Simultaneous Sampling for the sampling mode we can convert 2 independent analogue input signals simultaneously.

If Sequential Sampling is chosen only one multiplexed input channel (for example A) is converted at the time. By selecting Single Sequence Mjode (or “Start/Halt - Mode”) the Auto sequencer starts at the first input trigger signal, performs the predefined number of conversions and stops at the end of this conversion sequence then to wait for a second trigger. In continuous mode the Auto sequencer starts all over again at the end of the first conversion sequence without waiting for another trigger input signal.. The conversation mode is sequential and will post interrupt at the end of conversation meaning that it will stop converting analog data to digital until it receives a new trigger signal. Furthermore, ePWMxA (orange block in Figure 2.5.) should issue an interrupt request for the ADC unit to get a trigger signal from top layer of DSP program. Further discussion will come up in the next section where the main program will be explained in great details. For obtaining more information about C2000 F2833x ADC please see [14].

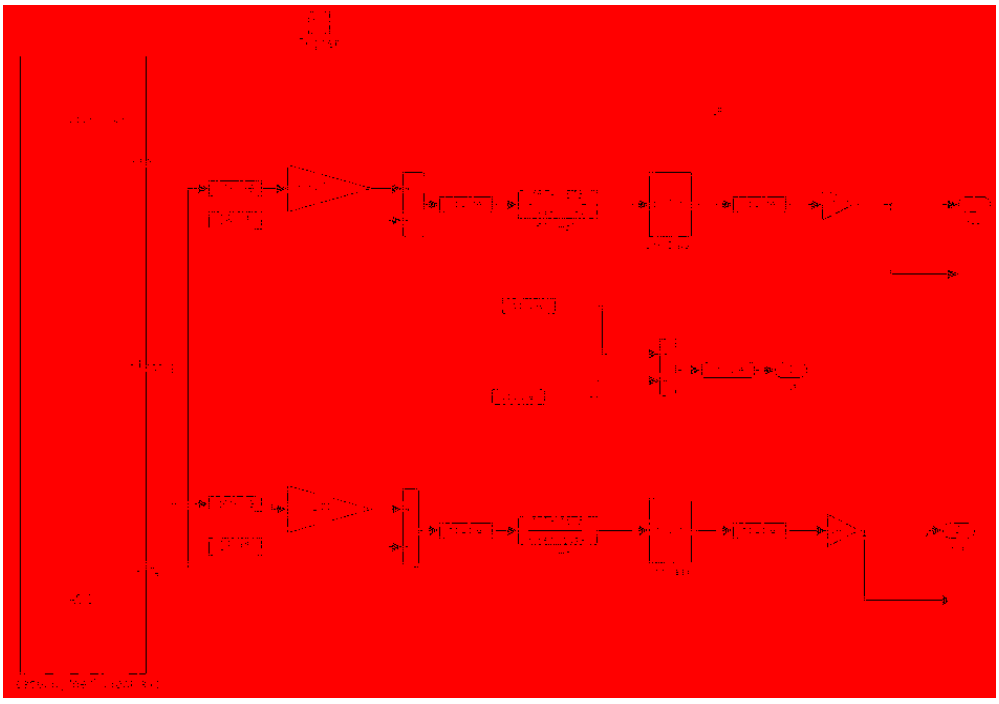

Figure 3.5. ADC subsystem implementing measurement and scaling

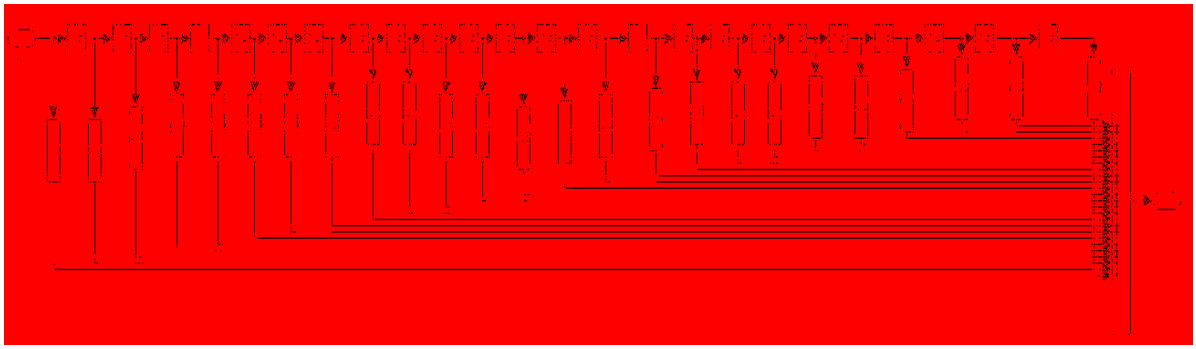

Figure 3.6. Unit delay implementation using 6 unit delay blocks

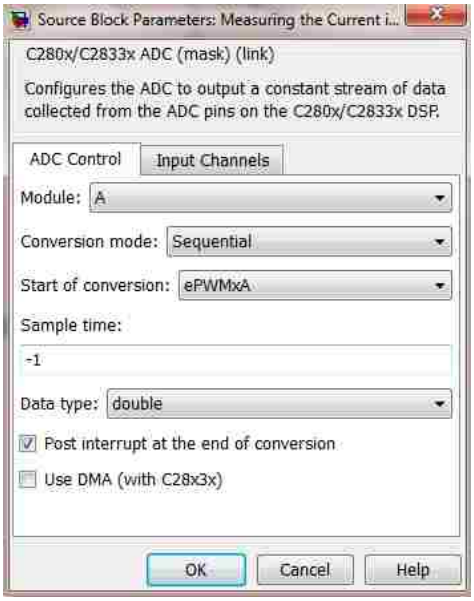

Figure 3.7. Show the properties of the ADC module

3.4. MAIN PROGRAM SUBSYSTEM

Figure 3.8 represents the main stabilized and efficient V/f algorithm implemented for a PMSM machine drive. For the sake of easiness in understanding the main functionality of the program, we explain the program in detail step by step.

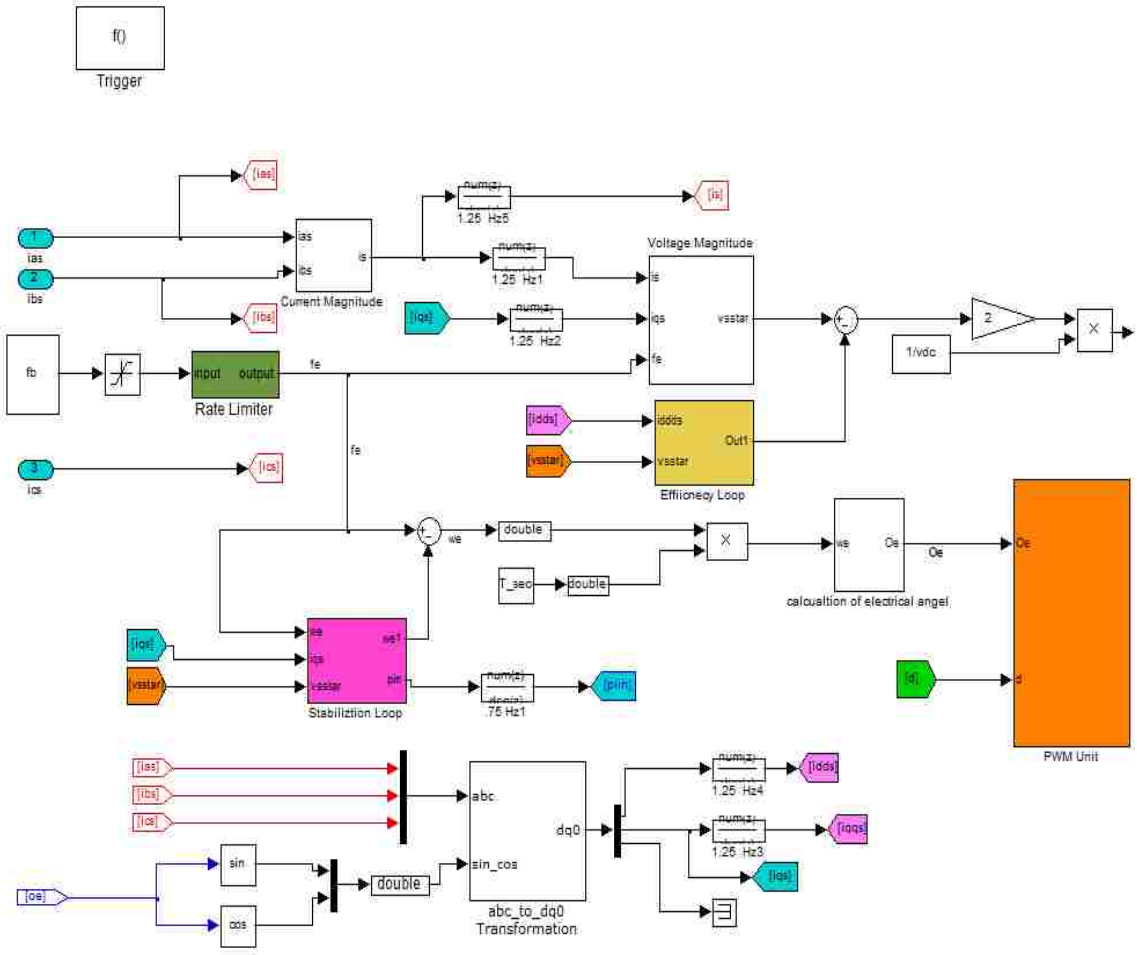

Figure 3.8. Implementation of sensor less stabilized efficient V/f for PMSM drive in Main Program subsystem

Since a sensorless method is being used, we should estimate the electrical rotor position from the commanded speed, but it is highly important for the reader to know that this angle is not necessarily same as the real rotor position. Therefore, it could be possible that the electrical angle is different than real rotor position, but in steady state value should be the same. In Figure 2.8, the parameter fb defines the maximum rotor speed as a step function, it is connected to an adjustable rate limiter controlling the desirable rise time of PMSM rotor. In here, the purpose of rise time is the amount of time rotor should spend to accelerate from zero speed to get maximum speed which is defined by fb. After

importing the electrical speed into the program, in the following the calculation of electrical angle is implemented which is shown in Figure 3.9.

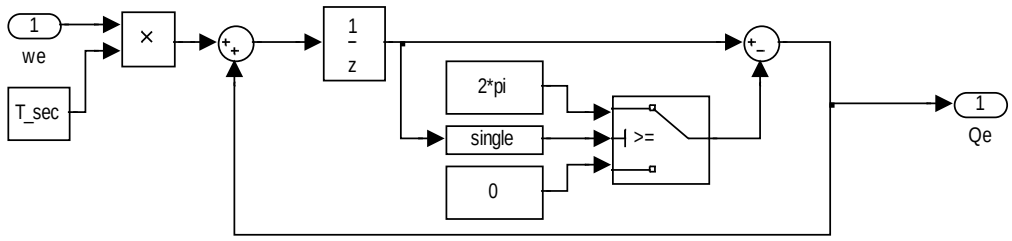

Figure 3.9. Calculating the electrical angle from the motor speed and program sampling time

The following equation is used in electrical angle calculation:

$$\theta_{e,t} = \theta_{e,t-1} + \omega_e T_{sec} \tag{21}$$

The unit delay will keep the previous sample point and send it for comparison unit. Using a switch block we can reset electrical angle whenever its value reaches 2π . The output will be electrical angle which will be used in other subsystems inside of the main program.

As it was discussed in the first section, voltage magnitude must be calculated from speed command and current magnitude which can be derived from following equation

$$V_s = I_s r_s \cos\phi_0 + \sqrt{(2\pi f_o \lambda_m)^2 + I_s^2 r_s^2 \cos^2\phi_0 - I_s^2 r_s^2} \tag{22}$$

Equation (21) is implemented inside of the voltage magnitude subsystem which is shown in Figure 3.10. It is noteworthy to mention here that all blocks have inherited (-1)

sampling time. The IF function block assure that all the time the term under square is positive. The assigned value for λ_m and r_s is presented in section 2 where all PMSM motor parameters is presented detail.

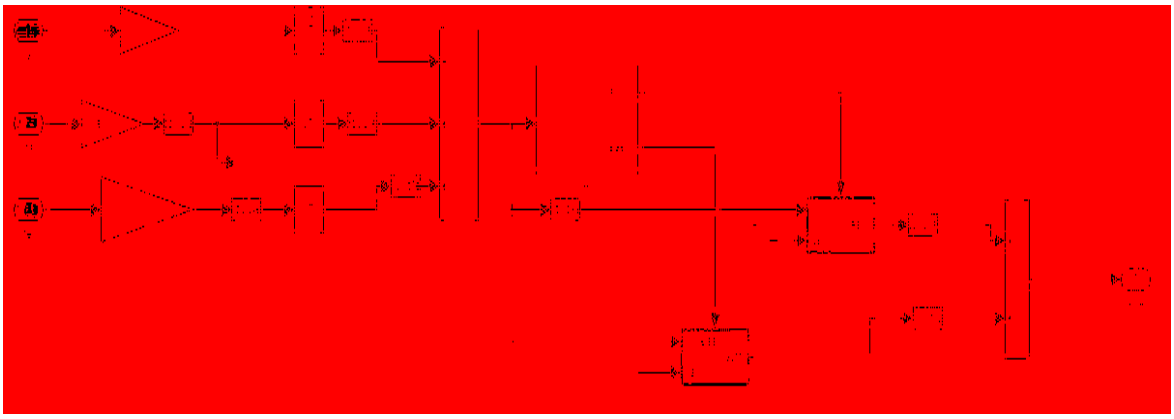

Figure 3.10. Finding voltage magnitude from frequency and a-b phases current

In equation (21), $I_s \cos\phi_0$ and $I_s \sin\phi_0$ are q and d stator current components which are calculated using abc/dq transformation block which is depicted in downside of the Figure 3.5. Finally, this block will give $I_q$and I_d which are critical parameters for V/f algorithm. As a matter of the fact the real and reactive power will be calculate using them and in the later part in which we implement efficiency loop, we will see that by regulatingI_d we can make it goes to zero. Figure 3.11 is showing abc/dq transformation and relevant equations.

Stabilization loop is also implemented based on the expected functionally which was described earlier in the first chapter. It must filter out undesirable DC component of the input real power in order to be capable of generating $\Delta\omega_e$, which is required for stabilization of PMSM, based on perturbation in the input real power. Figure 3.12 shows how $\Delta\omega_e$ is generated from AC portion of input real power and commanded speed.

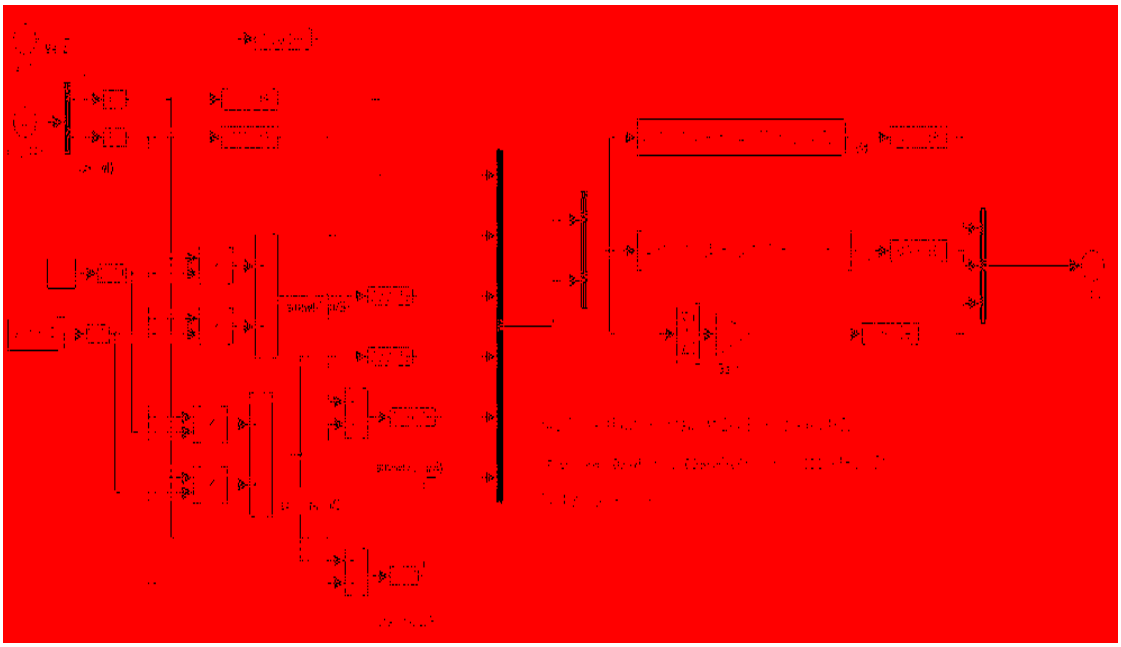

Figure 3.11. Park transformation

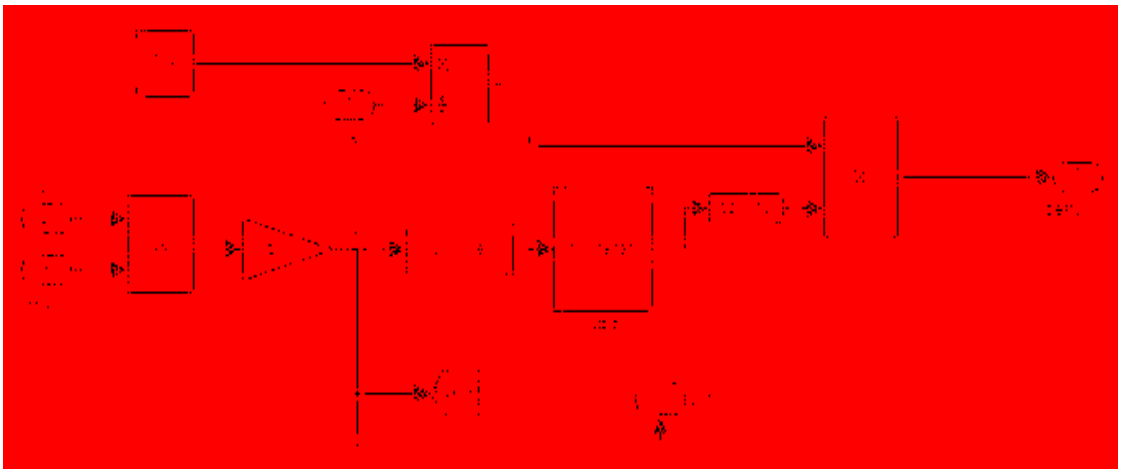

Figure 3.12. Stabilization loop implementation

Efficiency loop also is developed from the idea that by controlling the reactive power, I_d current can be controlled and set to the zero. A PI controller can fulfill the need

for this design goal where it compares reactive power magnitude with zero reference in order to adjust its value. PI controller parameters are found by try and error process which was so frustrating and time consuming. After running numerous tests for PMSM drive to verify the functionality of the efficient control loop. Figure 3.13 shows the efficiency loop implementation.

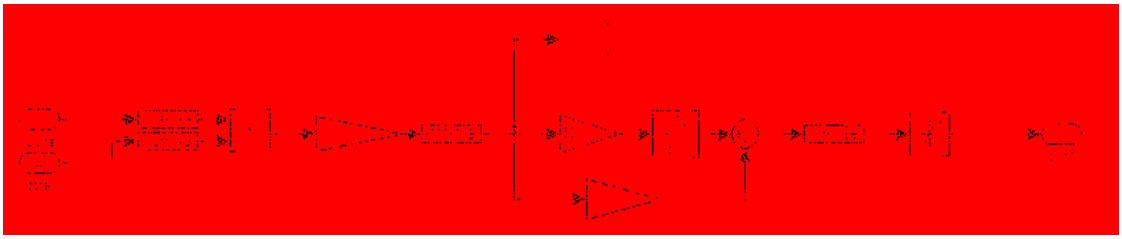

Figure 3.13. Efficiency loop implementation

3.5. EPWM UNIT

For the sine-triangle modulation, modulation index is calculated from $d = \frac{2\sqrt{2}V_s}{v_{dc}}$ where V_s is the voltage magnitude which is proportional to the electrical frequency and v_{dc} is dc power supply is connected at the input side of the inverter.

Figure 3.14 display how a Sine-Triangle PWM unit is implemented in the DSP program. The electrical angle and modulation index are inputs of this subsystem. By applying the PWM modulation, at the input side of multiplexer, the three signals $d_a, d_b and\ d_c$ get generated which h their duty cycle ratio range from -1 to 1 and are center round zero. Moreover, the three saturation blocks are used in the path between $d_a, d_b\ and\ d_c$ and multiplexer to limit and curb the allowable magnitude. Finally, the scaling is performed by adding a one to the duty ratios and dividing them by two which put their range between 0-1, and then multiply it by 7500 which is the period of the ePWM waveform.

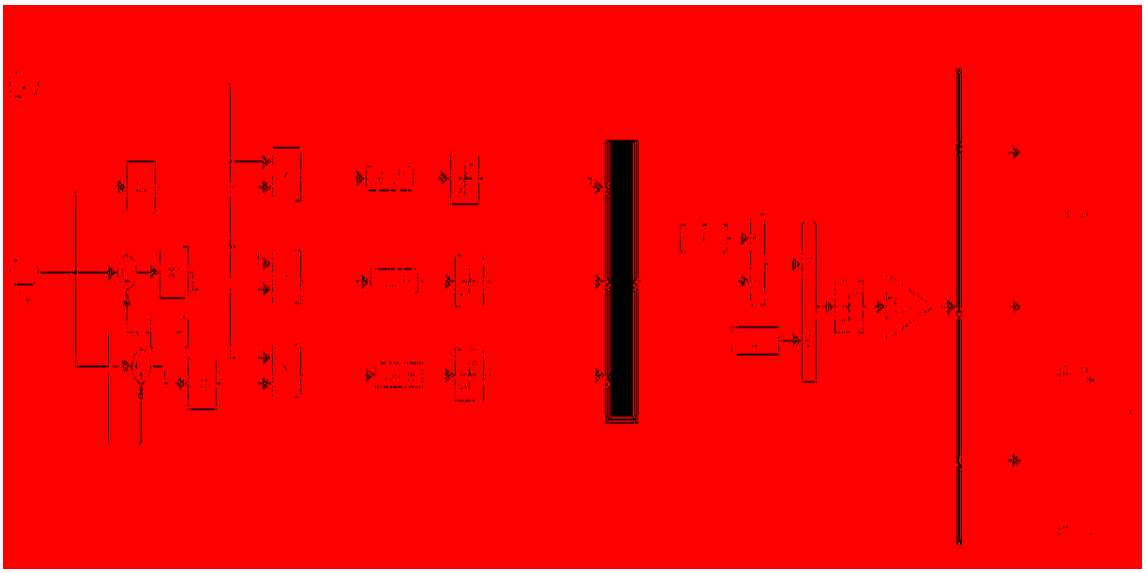

Figure 3.14. Display of ePWM unit inside of the main program

In machine drive application, it is common to choose switching frequency somewhere between 5 kHz-10 kHz, for this application chosen switching frequency is 10 kHz. It was mentioned earlier that the CPU clock is set for 150MHz inside of the F28335 eZdsp block, therefore in order to generate signal of 10 kHz at line ePWM1-6A, the TPRD which define signal frequency should be calculated from following equation:

$$\mathrm{TBPRD} = \frac{1}{2} \times \frac{f_{\mathrm{SYSCLKOUT}}}{f_{\mathrm{PWM}} \times \mathrm{CLKDIV} \times \mathrm{HSPCLKDIV}} = \frac{150\mathrm{M}}{2 * 10\mathrm{K}} = 7500 \qquad (23)$$

In the last equation, due to the fact that ePWM counting mode is set in Up-Down mode, a 2 factor is used in the denominator. The properties of the PWM block are shown in Figure 3.15. Here it is possible to set practically all features belonging to the PWM module of the F2833xin a simple graphical way. The controllable features ranges from setting of timer period, duty cycle, dead band generation, symmetrical/ unsymmetrical waveforms, to the control of then in the PWM cycle ADC conversations are to occur.

In Figure 3.15, left window shows a pane in which the basic ePWM settings needed to activate an ePWM unit are located. Register TBPRD defines the length of a

period of an output signal, in multiples of the time period of the input signal. Register CMPA which is abbreviation for compare value is important parameter cause the length of output ePWM signals become variable. Furthermore, two hardware signals ‘’SYNCI’’ and ‘’SYNCO’’ can be used to synchronize ePWM units to each other. For example, we could define one ePWM unit as a ‘’ master’’ to generate an output signal ‘’SYNCO’’ each time the counter equals to the period.

The ePWM counting mode can be adjust for 3 different modes of count up mode, count down mode and count up & down mode. Finally, since CPU clock frequency is too fast, 150 MHz, in order to make an independent clock source which is much slower than CPU frequency for ePWM, TB clock prescaler divider and High Speed TB clock prescaler divider should be used. All these settings are shown in Figure 3.15.

.

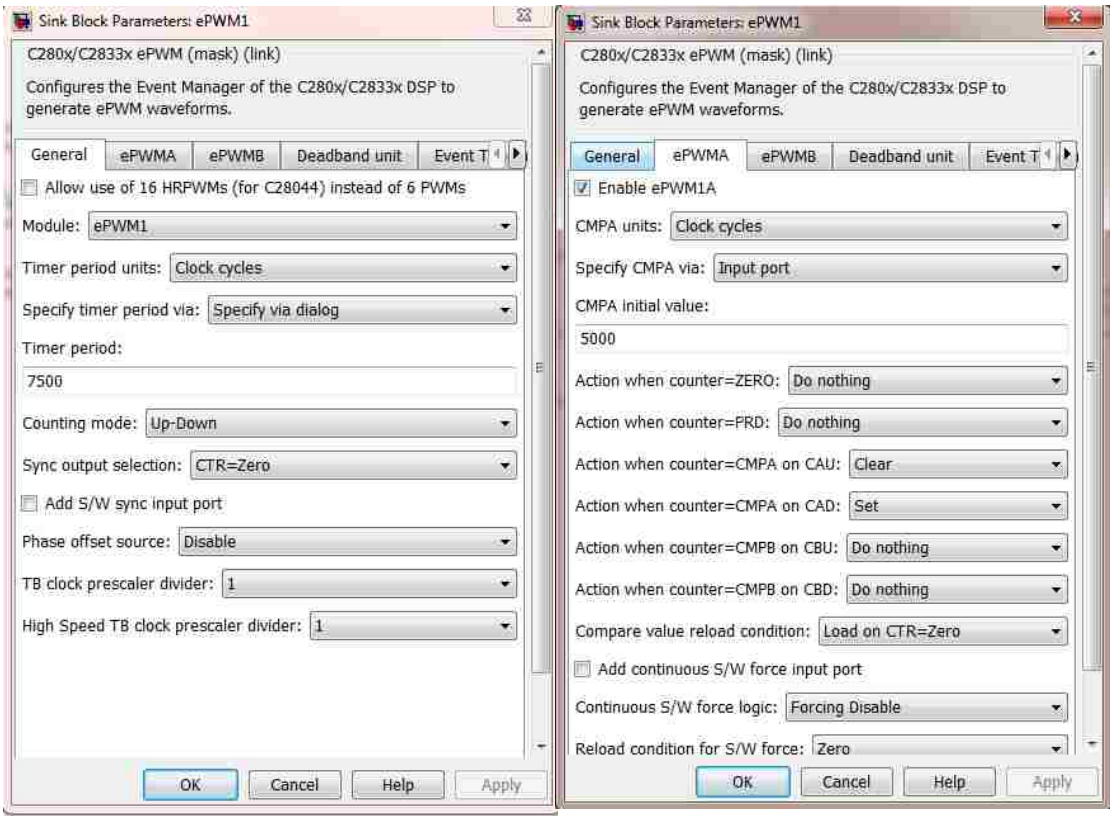

Figure 3.15. Property panels of ePWM unit

Furthermore, Right window in Figure 3.15 also show the action qualifier unit. Whenever the ePWM counter value reach to the compare value which is specified by CMPA register, the unit can change the value of the output signals Figure 3.16, the event trigger pane determine the source of the interrupt and manage interrupt request

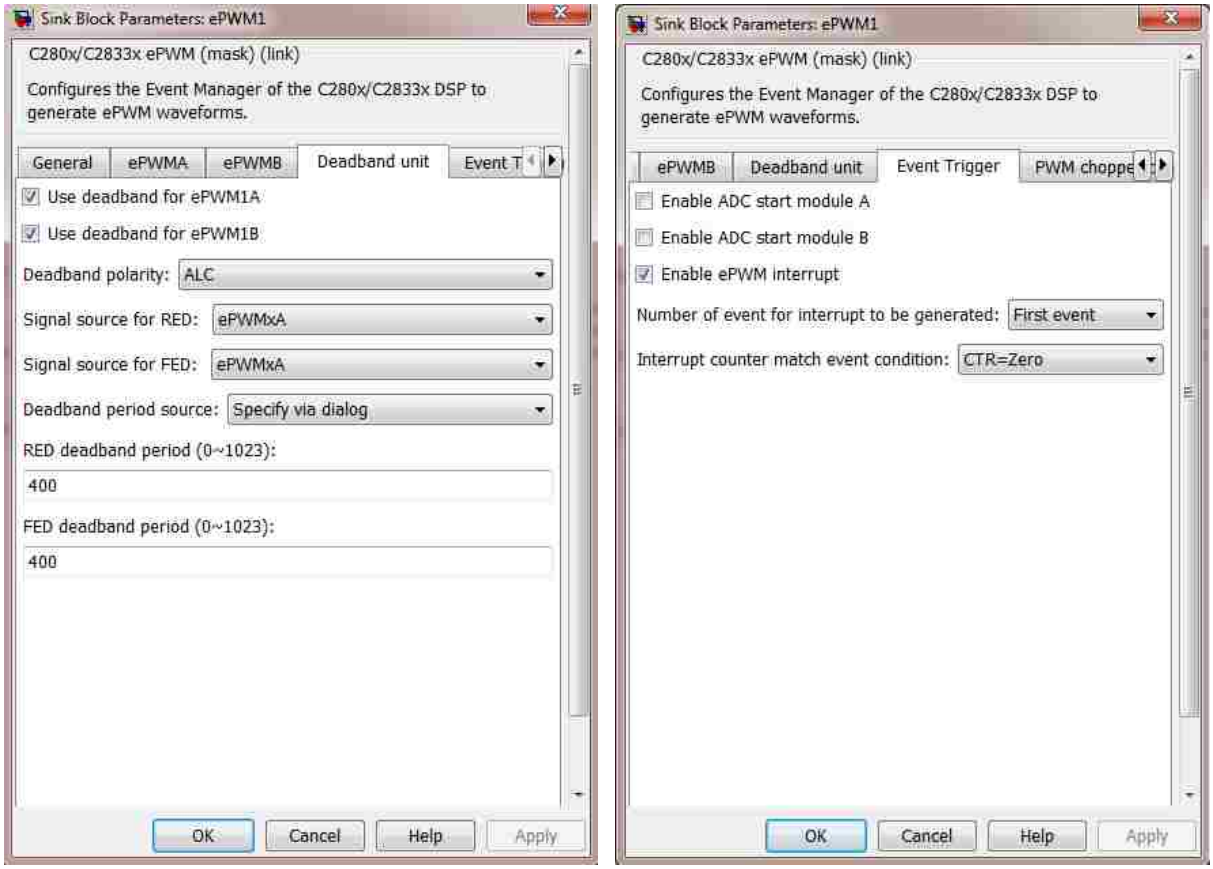

Figure 3.16. Property panels of ePWM unit

In switched mode power electronics, a typical configuration to drive a 3-phase system is shown in the Figure 3.17. A typical system consists of a 3-phase current or voltage injection circuit, in which a pair of power switches per phase is controlled by a sequence of PWM - pulses. A phase current flows either from a DC bus voltage through a top switch into the winding of a motor or via a bottom switch from the motor winding back to ground. Of course, we have to prevent both switches from conducting at the same

time. A minor problem arises from the fact that power switches usually turn on faster than they turn off. If we would apply an identical but complementary pulse pattern to the top and bottom switch of a phase, we would end up in a short period in time with a shoot-through situation.

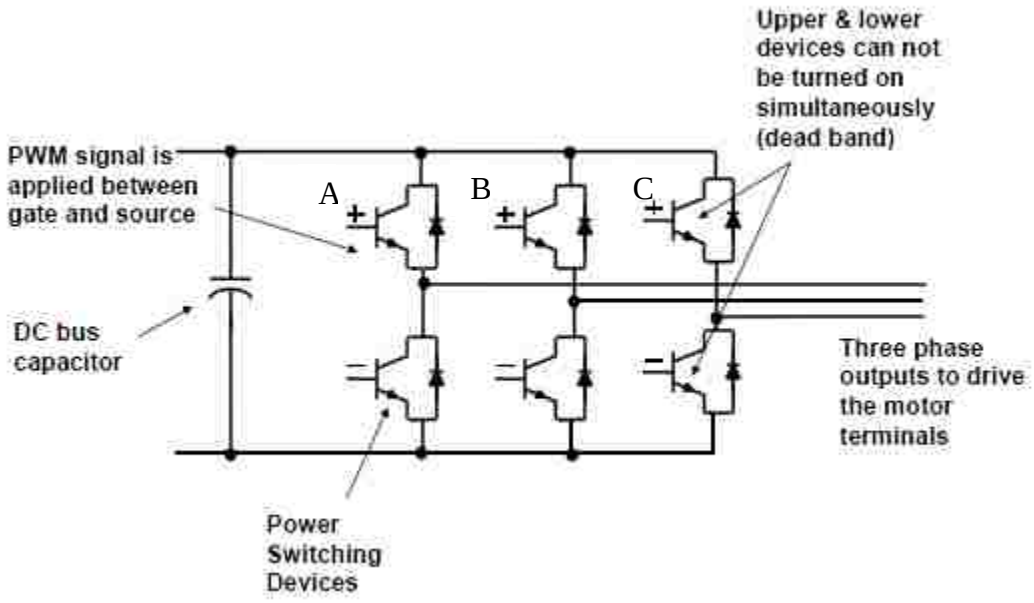

Figure 3.17. A typical configuration to drive a 3-phase system consist of a DC bus and 3- phase full bridge

Dead-band control provides a convenient means of combating current “shoot-through” problems in a power converter. “Shoot-through” occurs when both the upper and lower transistors in the same phase of a power converter are on simultaneously. This condition shorts the power supply and results in a large current draw. Shoot-through problems occur because transistors turn on faster than they turn off and also because high-side and low-side power converter transistors are typically switched in a complimentary fashion. Although the duration of the shoot-through current path is finite during PWM cycling, (i.e. the transistor will eventually turn off), even brief periods of a short circuit condition can produce excessive heating and stress the power converter and power supply. To address this issue, the best approach to shoot-through control separates transitions on complimentary PWM signals with a fixed period of time. This is called

dead-band. While it is possible to perform software implementation of dead-band, the F2833x offers on-chip hardware for this purpose that requires no additional CPU overhead. Compared to the passive approach, dead-band offers more precise control of gate timing requirements.

In Figure 3.18, complementary pulse sequences having different patterns can be selected from dead band polarity and dead band value will be defined using RED and FED registers. Figure 3.18 also contains all definable pattern can be used for different application. Finally, for getting more information about ePWM unit please see [15].

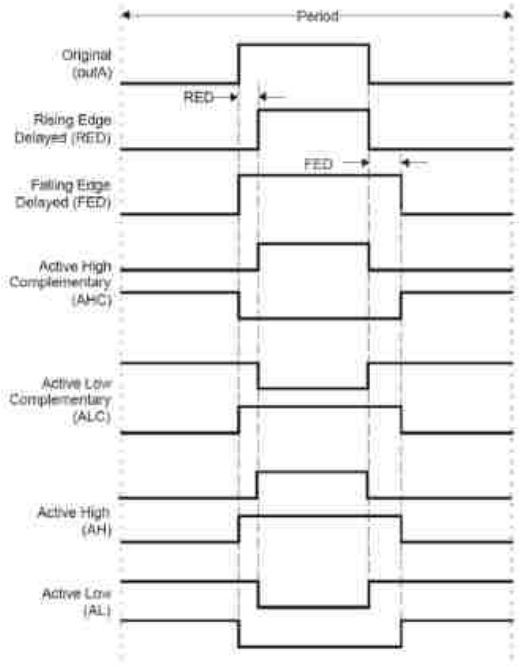

Figure 3.18. Dead-band waveforms for typical cases

3.6. ECAN UNIT

Finally, in order to see whether the proposed stabilized and efficient V/f control algorithm for PMSM is functional, some critical parameters like input real power, reactive power and q component of stator current need to be calculated and be compared for different cases where the stabilized and the efficiency loop may or may not be used.

Due to the fact that some of these parameters are math defined elements and also some other like input real power or reactive power cannot be measured by oscilloscope, user must be capable to communicate directly with DSP using one way from different defined communication protocol for DSP. The F28335 DSP supports three different communication protocols that can be used in communication between the DSP and Matlab. These are CAN, SCI and RTDX (Real Time Data Exchange). For these thesis, the CAN communication is selected due to its advantages it has over others communication methods. This portion of the thesis is dedicated to explain ECAN peripheral unit which was used in the DSP program.

3.6.1. Basics. Controller Area Network (CAN) is a serial network technology that was originally designed for automotive industry, especially for European cars, but has also become a popular communication protocol in industrial automation as well as other applications. The CAN bus is primarily used in embedded systems, and as its name implies, is a network technology that provides fast communication among microcontrollers up to real-time requirements which eliminate the need for the much more expensive and complex technology of a Dual-Ported RAM. It also grants high speed real-time communication and noise immunity in the noisy environment commonly found in a vehicle. [16] CAN is a two-wire, half duplex, high-speed network system, that is far superior to conventional serial technologies such as RS232 in regards to functionality and reliability and yet CAN implementations are more cost effective.
In general Controller Area Network has the following features:

- Is a high-integrity serial data communications bus for real-time applications
- Is more cost effective than any other serial bus system including RS232 and TCP/IP
- Provides better ease of use than any other serial bus system
- Operates at data rates of up to 1 Megabit per second
- Has excellent error detection and fault confinement capabilities
- Has the ability to function in difficult electrical environments
- Is now being used in many other industrial automation

A typical physical CAN bus consist of two wires terminated at both ends by 120 Ω resistors in addition to a reference wire. The system uses this three wire setup for differential signals for better noise immunity. The old and obsolete system used flat ribbon cables for communication; each cable was directly connected to its destination. The use of multi-wire systems leads to higher weight, higher cost, higher complexity and lower reliability due to the number of wires. Figure 3.19 displays a comparison between CAN bus set up and older multi-wire setup.

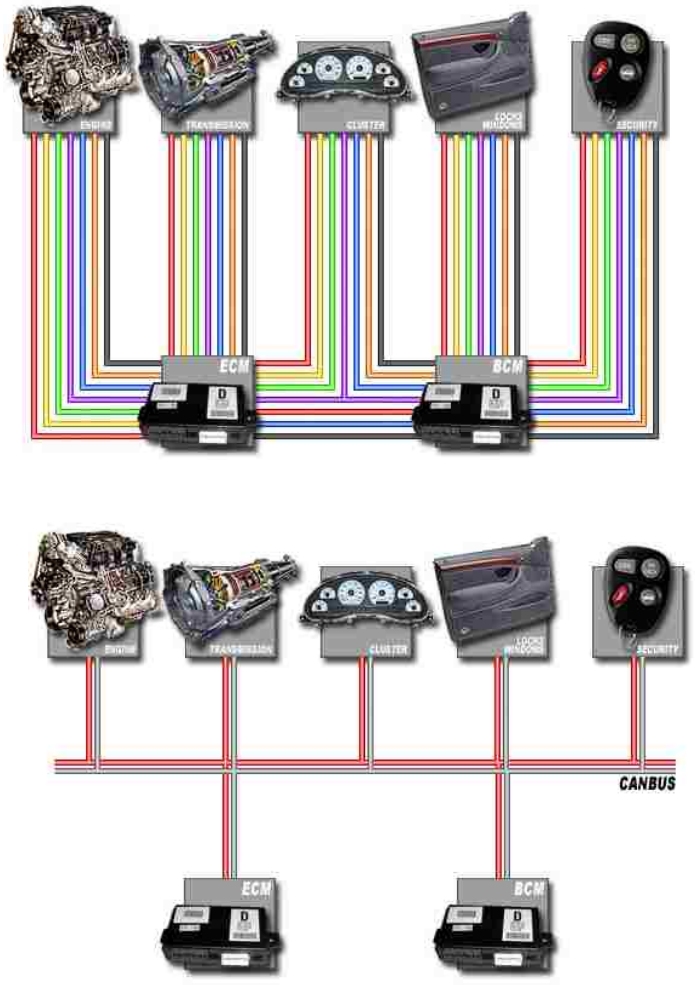

Figure 3.19. Comparison between older multi-wire setup and typical Can bus set up

So with this network system, each sensor or controller is now a node on the bus and can communicate to any other node on the network. Figure 3.20 shows a typical node setup, where the system have a CAN controller and CAN transceiver in each node. The CAN controller is where the message database is kept, which decodes and encodes all of the data being sent and received from that node to the network. The CAN transceiver actually transmits and receives the messages on the bus.

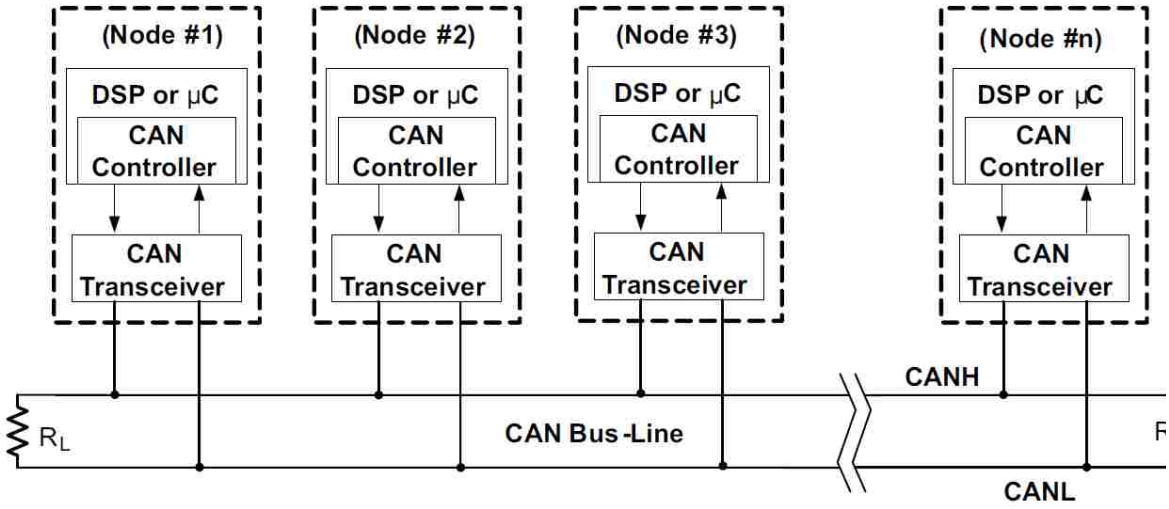

Figure 3.20. CAN node example

3.6.2. Message Frame Architecture. Various types of messages, or frames, exist in the CAN protocol. These types include: data, remote, error, overload, and inter space frames. Only the data and remote frames are set by the user, everything else is set by the hardware and come into the action whenever there is a fault or error on the CAN bus in order to protect form data accuracy and integrity. In Figure 2.21, standard data frame is shown, or message. Each message has a unique ID, a data field, and other header information.

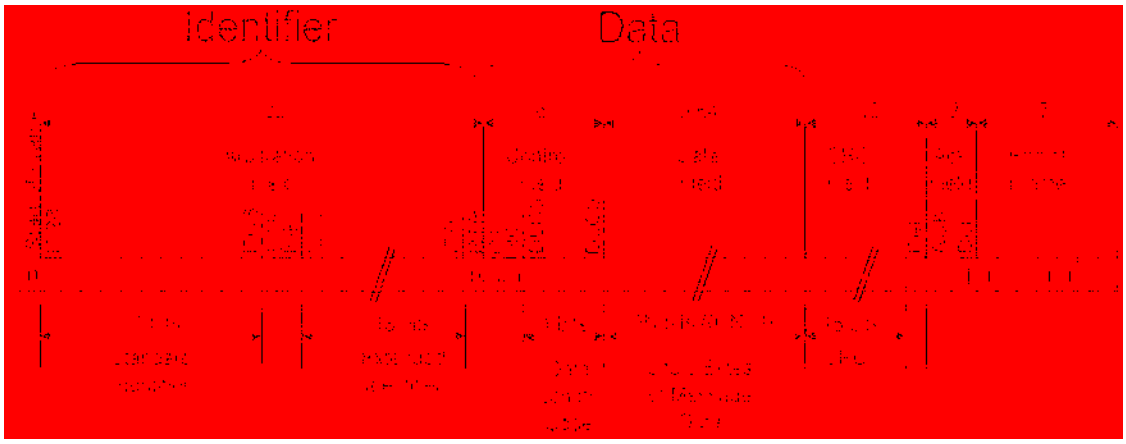

Figure 3.21. CAN data frame for 29-Bit extended format

- SOF (1 Bit)

The dominant Start of Frame (SOF) bit represents the start of a Data/Remote Frame. A CAN node, before attempting to access the bus, must wait until the bus is idle. An idle bus is detected by a sequence of 11 recessive bits (11 zero bits) which is the sequence of ACK Delimiter bit in the Acknowledgement Field (1 bit), the End of Frame Field (7 bits) and the Intermission Field (3 bits).(Figure 3.21)

- Arbitration field (12 or 32 bit)

The arbitration field contains of two components:

- 11/29 Bit Message Identifier, first Bit is MSB, and the CAN message ID can be 11 or 29 bits long. RTR (Remote Transmission Request) indicates either the transmission of a Data Frame (RTR = 0) or a Remote-Request Frame (RTR = 1).

A low message ID number represents a high message priority. For example, a message that its ID number is 0x000 must be the most important message in CAN database library which have the highest priority to access the CAN bus for data submission. The total length of the arbitration field is 12 bits when an 11 bit message identifier is used. As shown in picture 3, the total length of the arbitration field will be 32 bit with a 29 bit identifier

- Control Field (6 Bits)

The 4 LSB bits of the Control Field specify the length of the data block (DLC = Data Length Code), the MSB bit (IDE = Identifier Extension) indicates either standard 11-Bit format (Bit = 0) or 29-Bit extended format (Bit = 1). The Data Length Code (DLC) is normally set to a value between 0 and 8 indicating a data field length between 0 and 8 bytes.

- Data Field (8 Bits)

Data field is most important part of data frame message carrying information from different nodes of different subsystems. The data must be imported in hex format. As we will show in the later part, in real application, it is common t message o packed signals into a single message in order to minimize the message numbers defined for CAN database; therefore, the start bit of each signal is critical for a receiver node to easily distinguish and unpacked its relevant signals out of a specific message.

3.6.3. Message Broadcasting and Error Detection. The broadcasting of messages in a CAN network is based on a producer-consumer principle. One node, when sending a message, will be the producer while all other nodes are the consumers. All nodes in a CAN network receive the same message at the same time. Each node “listens” to the network bus and will receive every transmitted message on the CAN bus. The CAN protocol supports message filtering meaning that the receiving nodes will only react to data that is relevant to them and are defined in their database library otherwise nodes ignore the irrelevant messages. CAN assume that all messages are compliant with the defined standard and if they do not, there will be a corresponding response by all nodes in the network for Error Detection. If the consistency is not acknowledged by any or all nodes in the network, the transmitter of the frame will post an error message to the bus and will not grant permission to nodes for their message transmission. Moreover, If either one or more nodes are unable to decode a message, either detect an error in the message or are unable to read the message due to an internal malfunction, the entire bus will be notified of the error condition.

3.6.4. Canoe Software. Each node attached to the CAN bus needs a Host Processor, CAN Controller, and Transceiver in order to receive and send CAN messages. The Host Processor decodes the messages using a database which is defined by user to extract real data from received binary digits. For this project The Vector CANoe software along with a Vector CANcaseXL hardware interface was used to monitor and analyze the on-line operation of the CAN network. CANoe is a development and testing software tool from Vector Informatik GmbH. The software is primarily used by automotive manufacturers and electronic control unit (ECU) suppliers for development, analysis, simulation, testing, diagnostics and start-up of ECU networks and individual ECUs. Figure 3.22 shows inside of the CANOE software where the user can import any CAN database into the software which means that any message exist on the Can bus and is not defined for the CAN database cannot be motorized and be measured by the user. Moreover, I- Generator is a block in which user can manually define a CAN message out of the CAN data base library. As an example, the reader can imagine that in the DSP program where the user should define a commanded speed for PMSM, instead of using a constant Simulink block, it is possible to import CAN message from CANoe into the DSP program. Moreover, the user doesn't supposed to build a new DSP program for each new commanded speed, which is time consuming process, and he can simultaneously change the speed command while the DSP program is running to verify the V/f algorithm functionality for different speeds. The CAN database for the system was developed using the Vector CANdb++ software. The CANdb++ is a data management program which can be used to create and modify CAN databases. The CAN Controller stores received data bits serially until an entire message is available and then transfers it to the Host Processor. The Transceiver acts as a voltage level shifter and adapts signal levels from the bus voltage level to the voltage level that the CAN controller expects. For further information about making up a CAN database using CANdb++ and setting up the CANoe software for monitoring the CAN messages, please refer to the following references [17, 18].

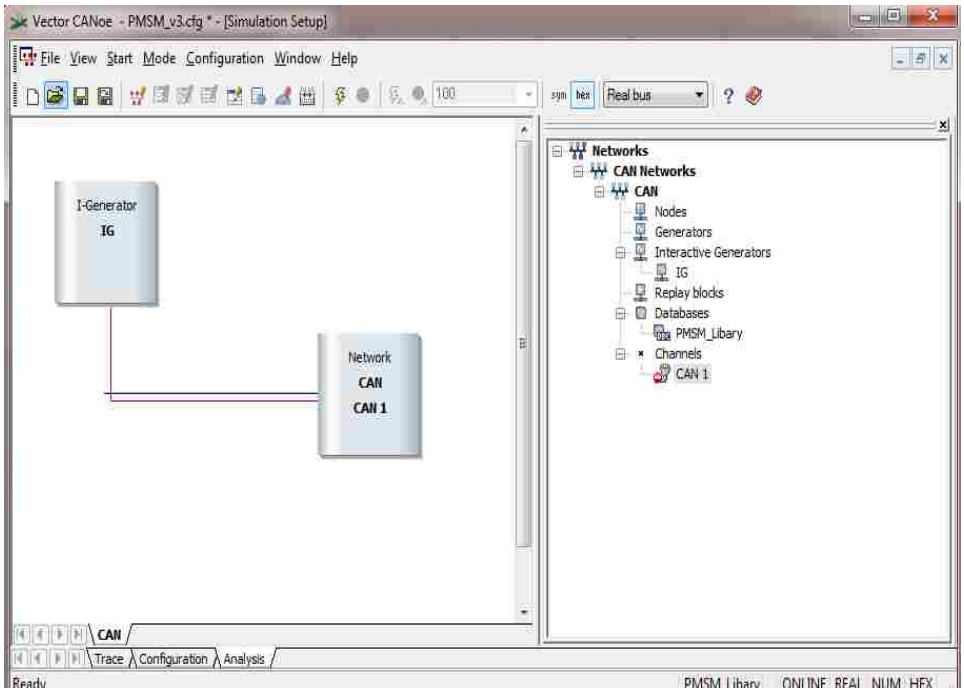

Figure 3.22. CANoe configuration window

3.6.5. Can Using Simulink's Embedded Coder. This section will provide a basic guide to get the F28335 DSP programmed to use CAN using Simulink's embedded coder. As a first step the user is supposed to set a baud rate which he has already defined for CANoe software. By opening up the target preferences block in Simulink and navigating to the eCAN_A section under the Peripherals tab the baud rate can be define for the CAN bus, as shown in Figure 3.23. To get idea about how to set a particular bite rate please see the reference [12].

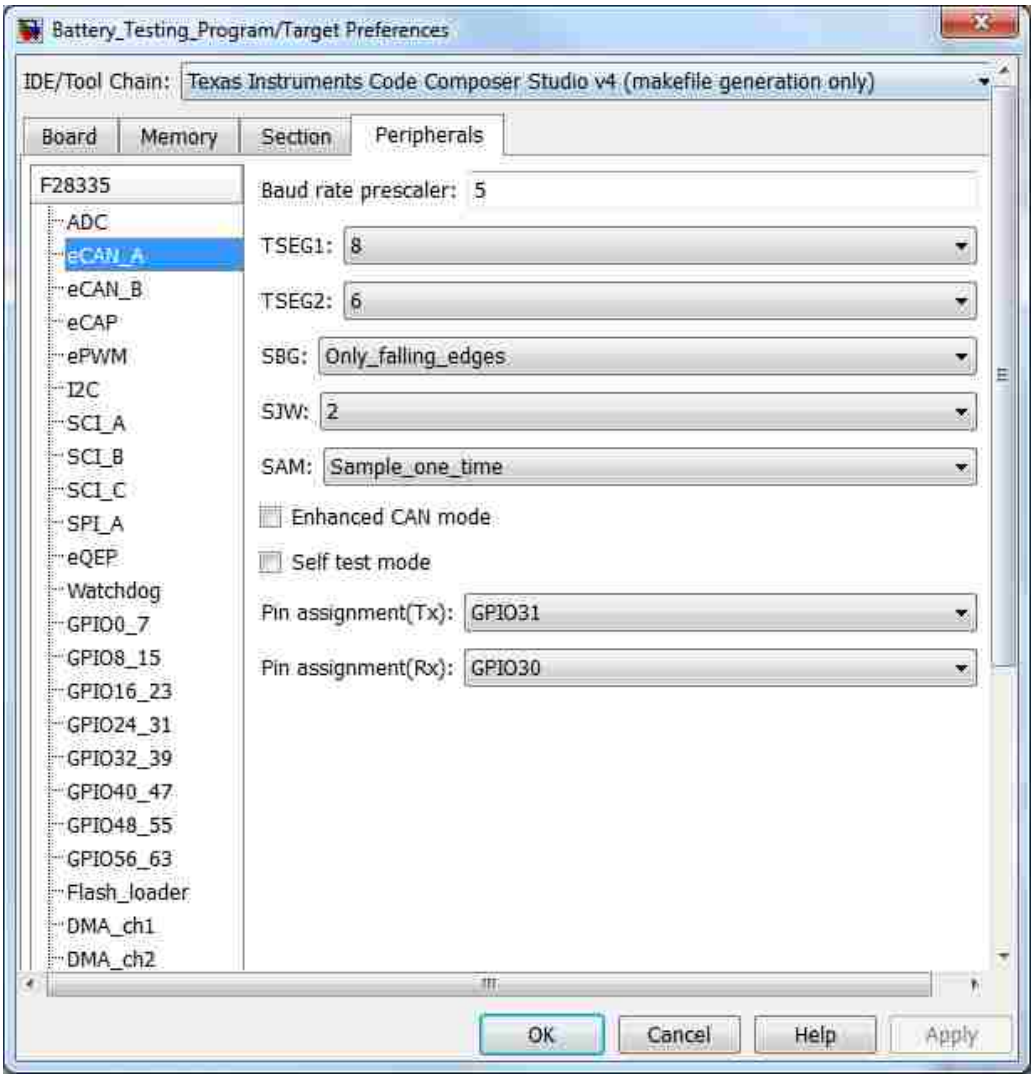

Figure 3.23. CAN A preferences

Next users need to setup the Vector CANcaseXL box ,Figure. 3.24, to operate at a 1 Mbps baud rate as well. To do this, please hook up the box to the PC and open the Vector Hardware application. Backing to the Figure 3.22, by double clicking on the Network can bus; the baud rate can be also defined for the software. Finally a CAN harness 2 wire cable attached to the 9 pin D-sub pin out which is shown in figure 3.25 should be connected between DSP and CAN vector box.

Figure 3.24. Vector CAN box

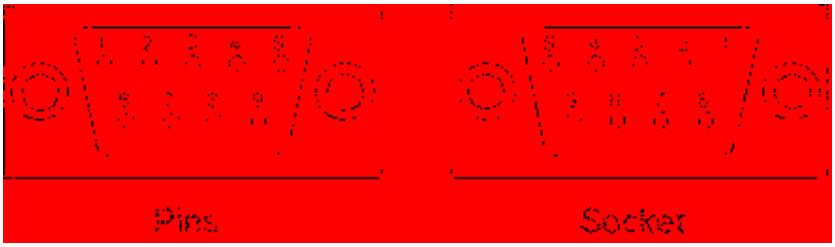

Pin Nr.	Signal	Description
1	-	Reserved
2	CAN_L	CAN Bus Signal (dominant low)
3	CAN_GND	CAN ground
4	-	Reserved
5	CAN_SHLD	Optional shield
6	GND	Optional CAN ground
7	CAN_H	CAN Bus Signal (dominant high)
8	-	Reserved
9	CAN_V+	Optional external voltage supply Vcc

Figure 3.25. D-sub pin out

CAN communication with Embedded Coder is done using four blocks: CAN Pack, CAN Unpack, eCAN Transmit, and eCAN Receive. The first two blocks are found in the Target Communication submenu of the C2000 branch in Simulink's library browser. The latter two blocks are found in the C28x3x submenu. The CAN Pack block (Figure 3.26) takes Simulink values and packs them into a message that is transferred over the network using the eCAN Transmit block. If the user be lucky enough to be using a 32-bit version of Matlab/Simulink there is an option to load the .dbc file you created earlier to fill in all these options; otherwise you have to fill them in by hand.

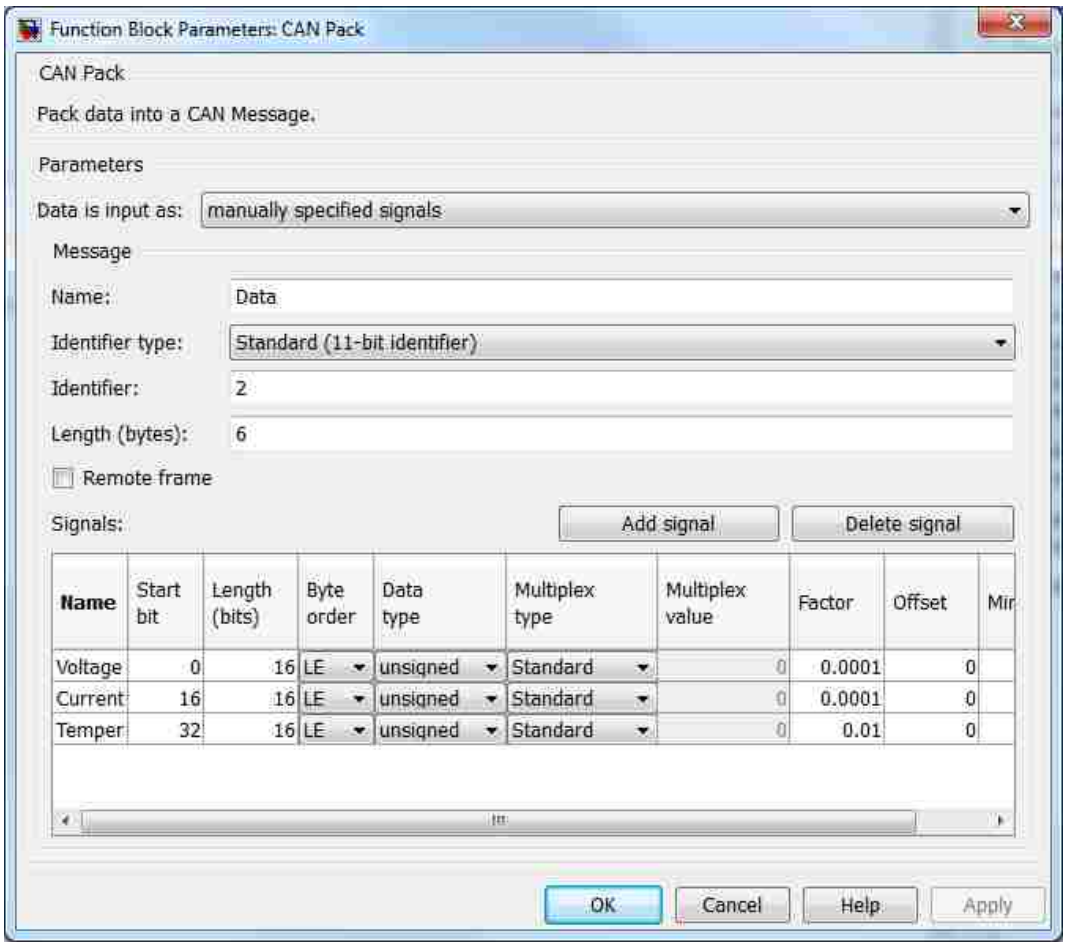

Figure 3.26. CAN Pack Block

By selecting “manually specified signals” from the “data is input as” drop-down menu then all the information you enter has to match what was entered into your database file.

The eCAN Transmit block settings are also pretty straight forward. The dialog menu shown in Figure 3.27 should have similar setup options to what you will be using. Mailbox number is a given number from 1-12, and it can be random number. The user can choose between the A and B CAN bus. The message identifier should be the same message ID in hex, minus the “0x” from the database file which was defined by CANdb++ and was imported into the CANoe software. The box ‘’ post interrupt when message is transmitted’’ should also be checked [15] help to set up a eCAN unit for DSP.

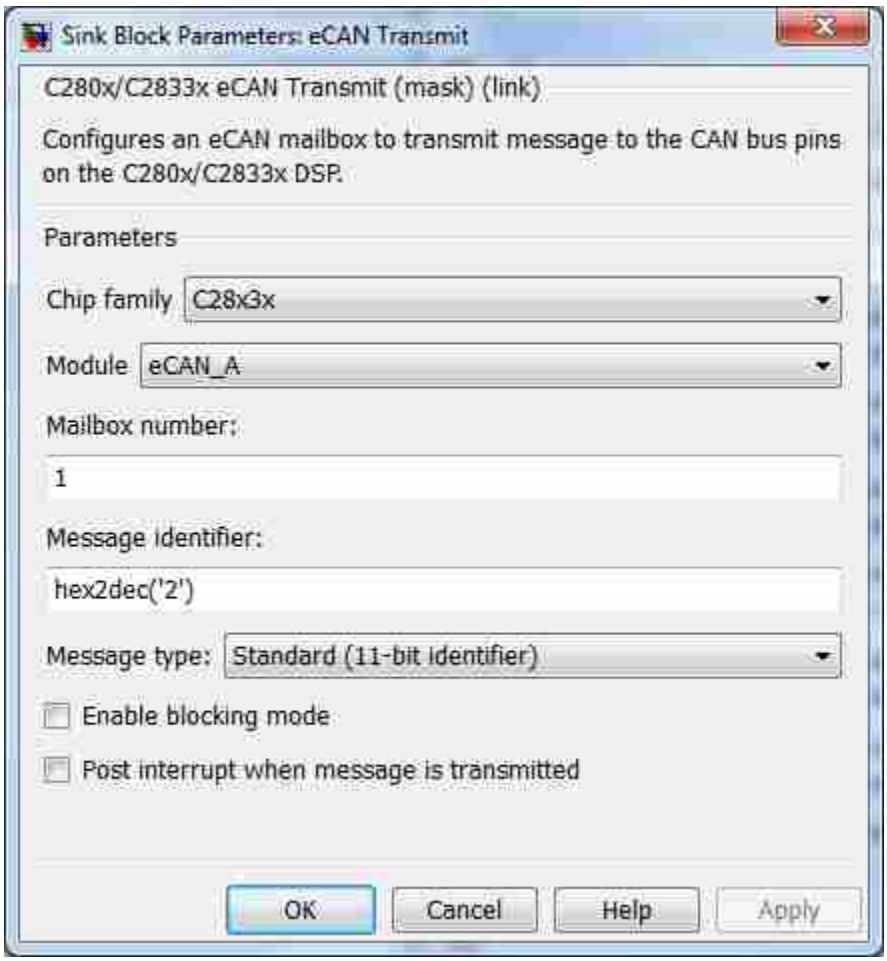

Figure 3.27. eCAN Transmit block

4. SIMULATION AND EXPERIMENTAL RESULTS

4.1. SIMULATION

In order To verify the accuracy and performance of the both stabilized loop and proposed efficiency-optimizing control technique, simulation tests have been conducted using the Simulink of the MATLAB. The PMSM parameters used in the simulation is presented in the table 2.2.

Table 2. 2. PMSM motor parameters which were used in experimental tests

$L_d = L_q = 1.9mH$	$Rated\ Power = 15\ Kw\ \ rated$
$\lambda_m = \ .278$	$Speed = 1750\ r/min$
$J = 15 * 10^{-3} kg.m^2$	number of poles= 6
$B_m = 20.4 * 10^{-3} N.m.s$	r_s= . 149
I_{rated}= 50 A	

As it was discussed in the first chapter, PMSM motors that are not equipped with damper winding have serious stability problems during transient conditions like for example, during time motor start up , the rotor may capable to drive out from zero speed, but before reaching to the commanded speed it will lose synchronization. Another common instability scenario is when the amount of load torque exerted on PMSM rotor shaft suddenly and abruptly get changed, commonly happen in field of motor application leading motor into the instability situation. Therefore, the first test is to examine the effect of stability loop on the PMSM start up using stabilized loop. Figure 4.1 shows the measured rotor speed of the machine, when the machine is ramped up to different frequencies under no load, for the sensorless V/f controller where the stabilization loop is not utilized From Figure 1.3, the stable operation of the machine at low frequencies and the unstable operation at high frequencies is evident, as expected from the stability analysis and the loci diagram was shown in Figure 2.5.

The same test was carried out with the drive configuration shown in Figure 2.6, with the stabilizing loop in the system. The stabilizing loop parameters which were used to calculate the eigenvalue plots in Figure 2.5 were used in the drive system. Since the stable operation of the machine was possible at low frequencies the stabilizing loop was added to the system. Figure 4.2 shows the results. Comparing this figure with Figure 4.1, the effect of stabilized loop should be tangible for the readers indicating stabilization loop is correspond to the damper winding on rotor cage of synchronized electrical machines.

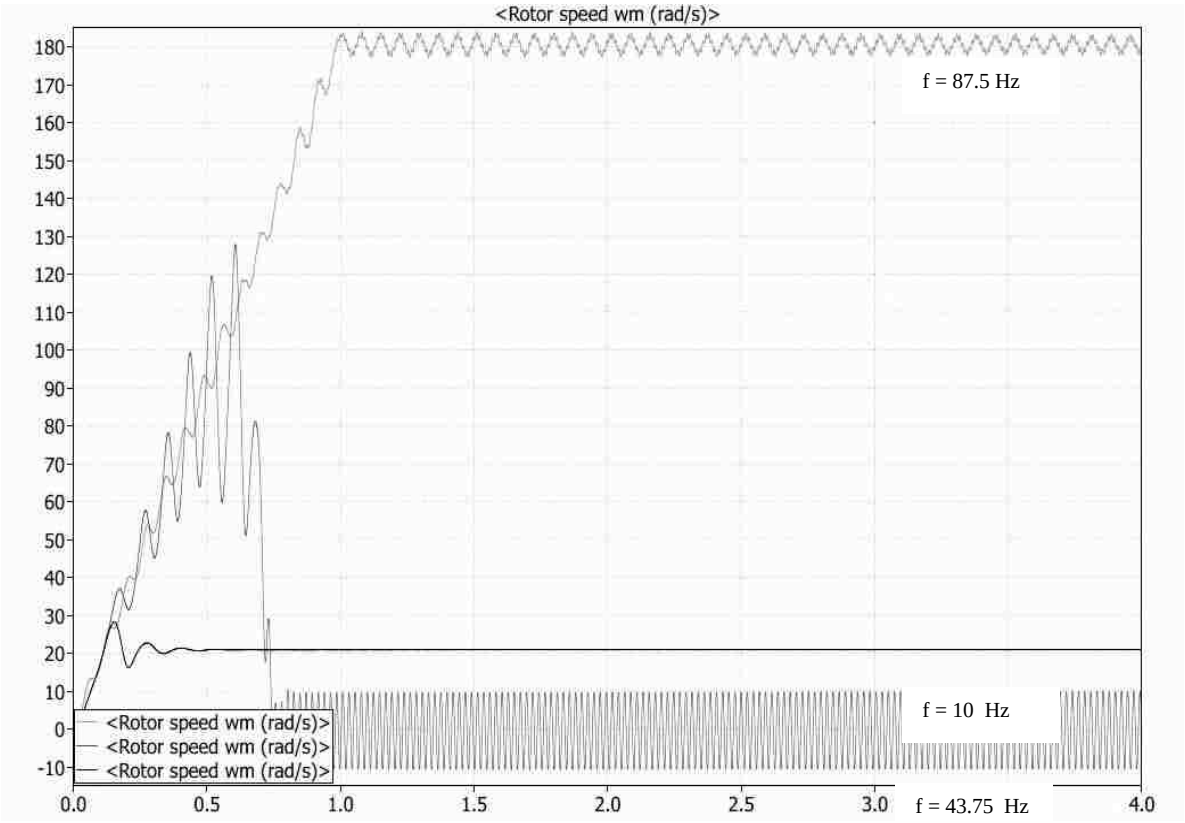

Figure 4.1. Measured rotor speeds at different frequencies, under no load, without stabilizing loop in the system

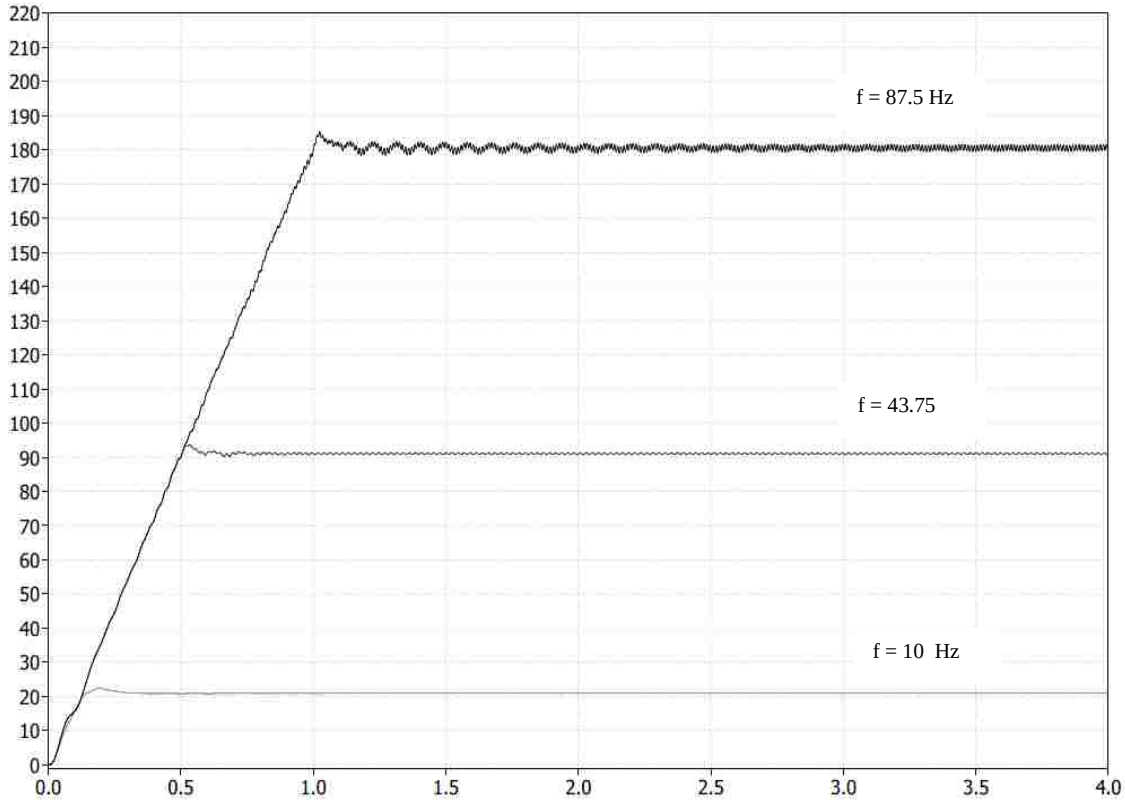

Figure 4.2. Measured rotor speeds at different frequencies, under no load, with stabilizing loop in the system

In the next simulation test, the effect of adding efficiency loop to a stabilized V/f sensorless control method for PMSM is studied by measuring various motor parameters for two different scenarios. In the first case, a stabilized V/f is not utilized with efficiency loop while in the second test efficiency loop is employed in control loop.

In the first scenario, the machine is started at zero speed and load torque, it then ramps up the speed towards half of the rated value, which corresponds to an electrical frequency of 98.43 Hz which is equivalent to 940 rpm. At t = 3 seconds, the load torque is stepped to the rated value of 15 N.m. Later on, at t=5 the load torque magnitude increase to 25 N. Finally, at t = 7 seconds, the load torque is stepped back to zero. The simulation results are presented in Figures 4.3 - 4.9 and in all these figure the green line diagram represent the results of test in which efficiency loop is employed.

Figure 4.3, support our earlier claim that by controlling the reactive power and keeping its value to the zero, we should able to see changers in magnitude of input real power. It is noteworthy to mention that as the amount of load torque applying on motor shaft increase, the magnitude of input real power increase consequently and the benefit of using efficiency loop become more apparent due to the fact that power losses get much smaller compare to the low and light load torque. By making comparison between 2 diagrams in Figure 4.3, it is clear that by using the second method, it is possible to save up the input power up to the 10%, and reduce the machine losses. Because the *q*-axis current is directly proportional to the electrical torque, zero *d*-axis current means that the stator current magnitude is at its minimum. Moreover, Base on the result presented in Figure 4.5, in order to control the reactive power, the voltage magnitude need to be regulated. In fact, in any type of synchronized machine starter voltage magnitude is proportional with reactive power.

Base on simulation results of Figure 4.7 and 4.8, at 25 N.m torque, the *q*-axis current has a significant magnitude. However, the *d*-axis current is also very large, even though it does not have any contribution to torque generation, and it cause inclination in power loss, but in the next test, the efficiency optimization algorithm is added to the simulation and the same test procedure is followed as in the first test. Comparing results in Figure 4.7 has almost identical waveforms for rotor speed, torque, and *q*-axis stator current. One of the differences lies in the waveforms of the *d*-axis current, which is maintained at near zero in Figure 4.8.

Finally, as can be seen from Figure 4.9, after the speed ramp, the motor is able to maintain a constant speed even with large step changes in load torque. The operation is stable in the whole speed and torque range regardless of efficiency loop usage in the control loop. In all following graphs, the green color one shows the stabilized V/f which efficiency loop controller is employed while the blue one represent the stabilized V/f without efficiency loop controller.

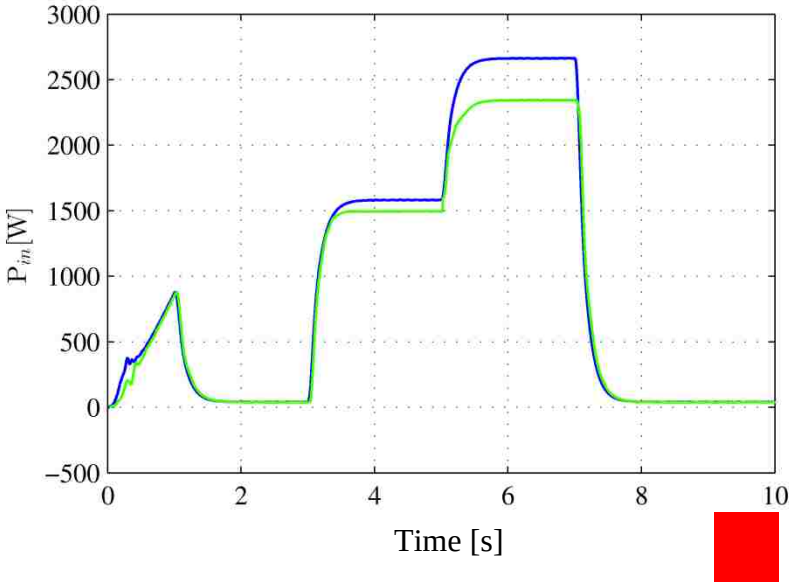

Figure 4.3. Comparison of input real power

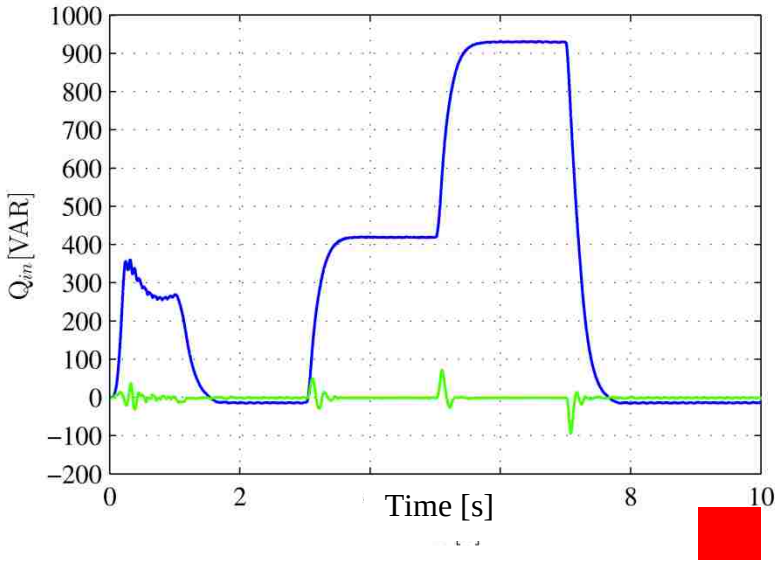

Figure 4.4. Comparison of input reactive power

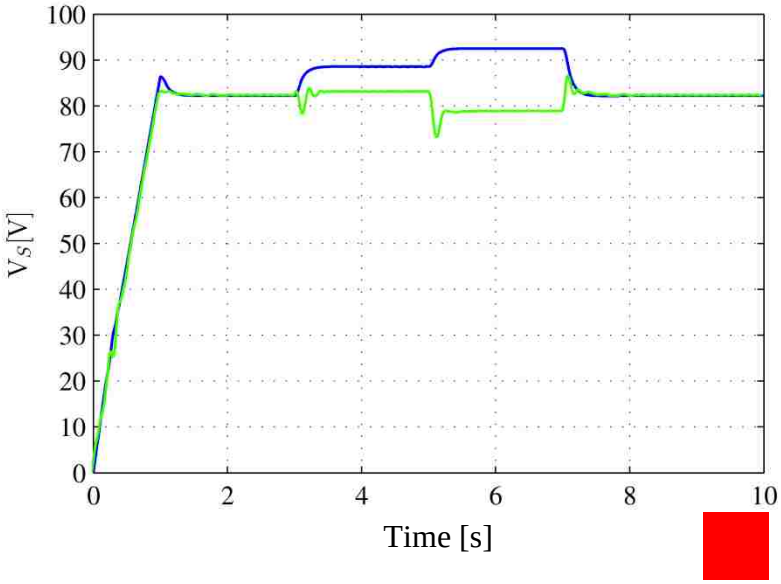

Figure 4.5. Comparison of stator voltage magnitude

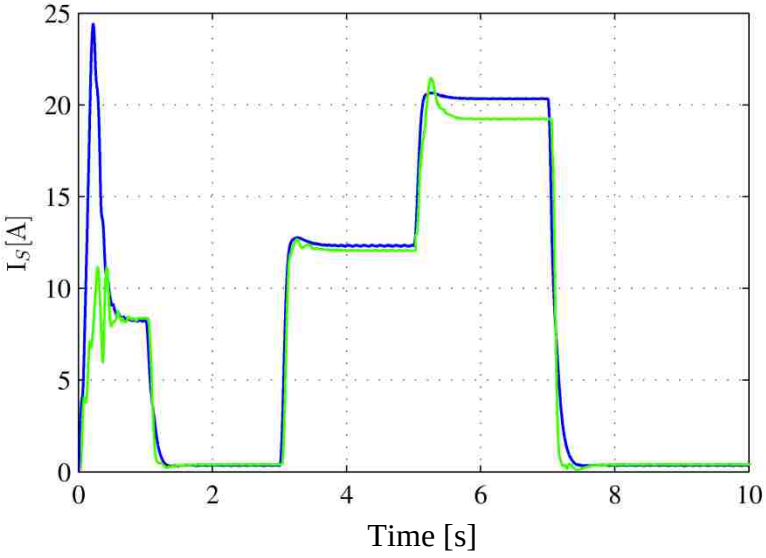

Figure 4.6. Comparison of stator current magnitude

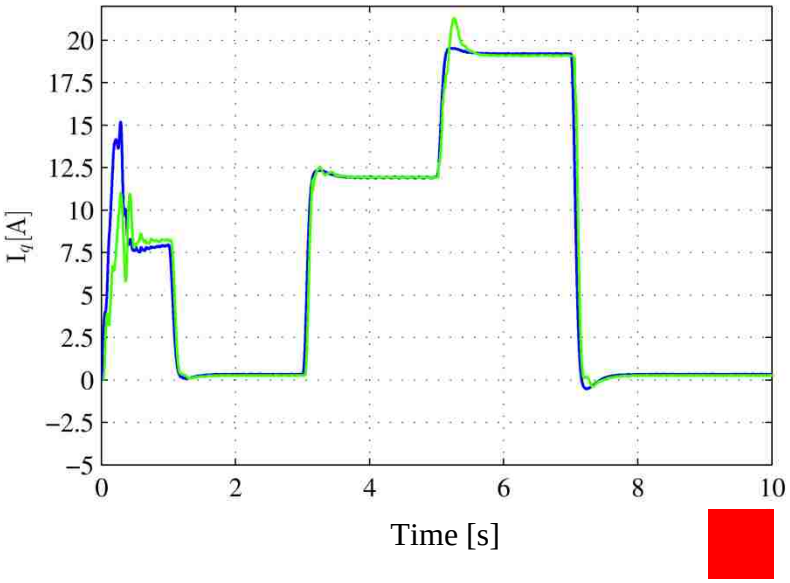

Figure 4.7. Comparison of stator current q component

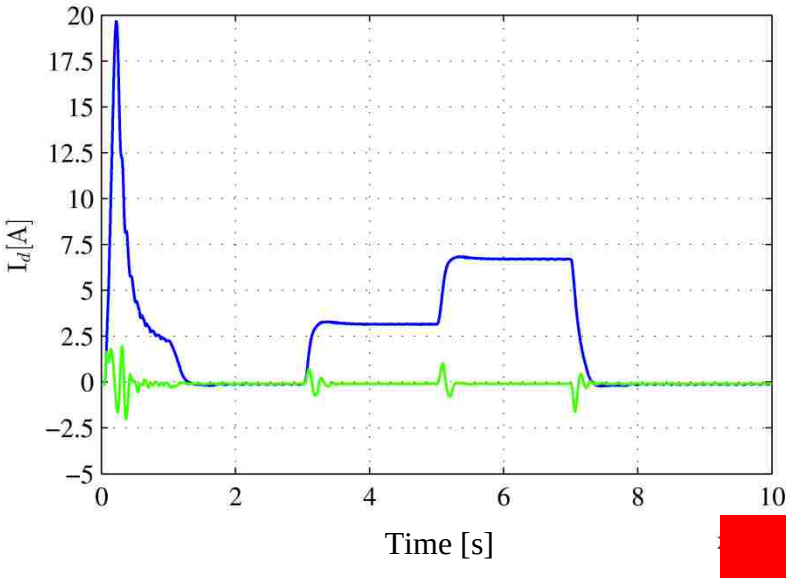

Figure 4.8. Comparison of stator current d component

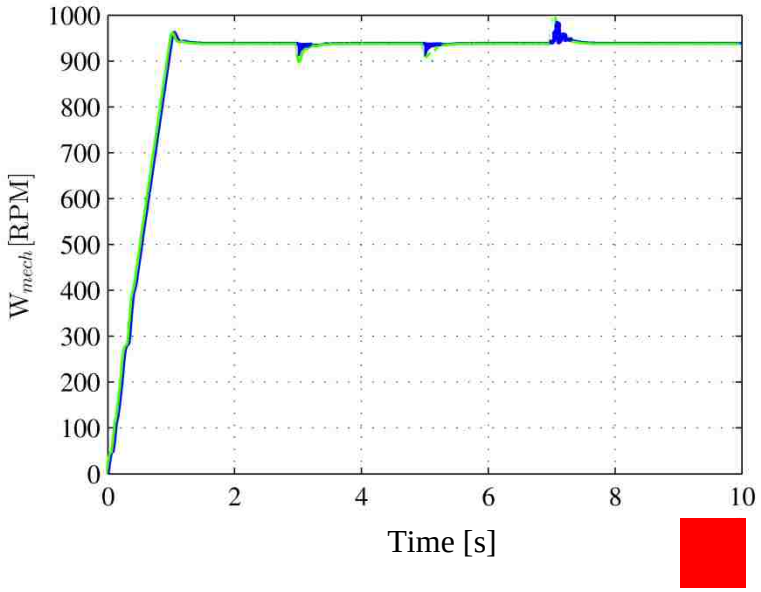

Figure 4.9. Comparison of rotor mechanical speed

4.2. EXPERIMENTAL RESULTS

Figure 4.10 and 4.11 show the lab experimental set up for this thesis. The Matlab 2012 has been installed on the lab computers with all the toolboxes and subsystems which are required for C2000 DSP rapid prototyping. Moreover, the dc motor is driven by a DCS800 ABB drive while the PMSG drive is a custom made drive built by the team using a TMS320F28335 DSP from Texas Instrument and a Semikron SKS 83F B6CI 44 V 12 inverter.

To be able to run PMSM and control it based on the program running on its DSP, a 320 V dc supply must feed the PSMSM drive which is provided by constant dc power supply shown in Figure 4.10. Both PMSM drive and DC drive support the CAN communication, and the PMMS calculated and measured motor parameters are read out of the CAN port was integrated into the PMSM drive. Furthermore, it was very crucial for the experimental tests that being able to apply load torque on PMSM shaft abruptly to examine the dynamic behavior of PMSM machine under heavy load torque changes while a sensorless V/f is supposed to control its speed. For this purpose, Advanced

DCS800 ABB drive allow the user to communicate with dc machines by reading dc machines measured signals like mechanical speed or by sending the user command such as load torque ,which is our primary concern in this case, through the CAN protocol communication.

Figure 4.10. Lab set up for efficient and stabilized V/f for PMSM machine

Finally, the experimental results are presented in Figures 4.11 – 4.18, all the signals are measured and recorded in CANOE software originally, but to improve result quality and make it more appealing for the readers the recorded data was transformed into the Matlab and was plotted regain. In all following graphs, the green color one shows the stabilized V/f which efficiency loop controller is employed while the blue one represent the stabilized V/f without efficiency loop controller.

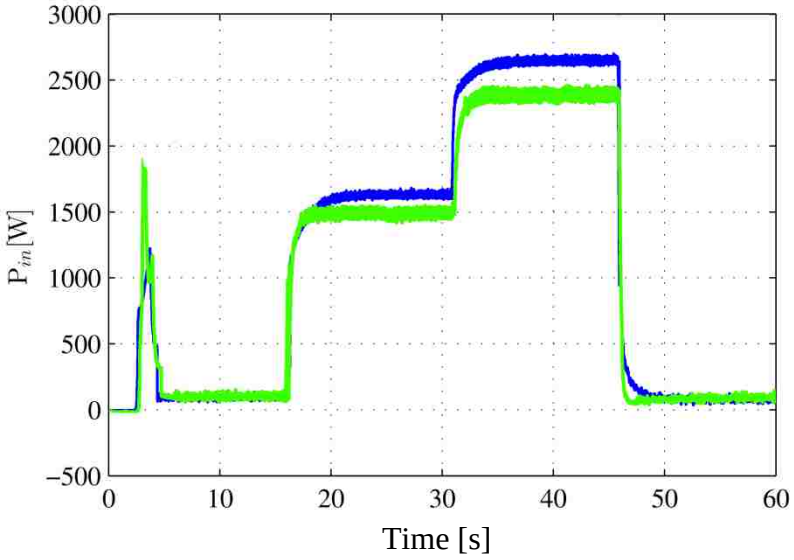

Figure 4.11. Comparison of input real power

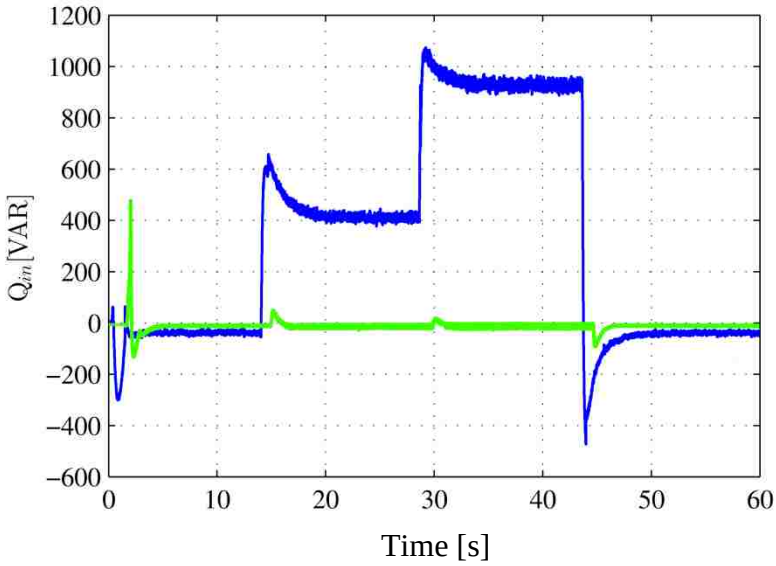

Figure 4.12. Comparison of input reactive power

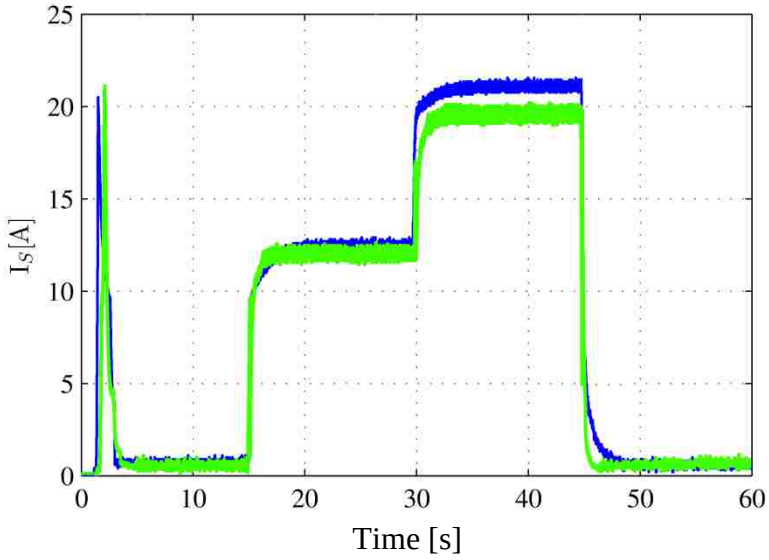

Figure 4.13. Comparison of stator current magnitude

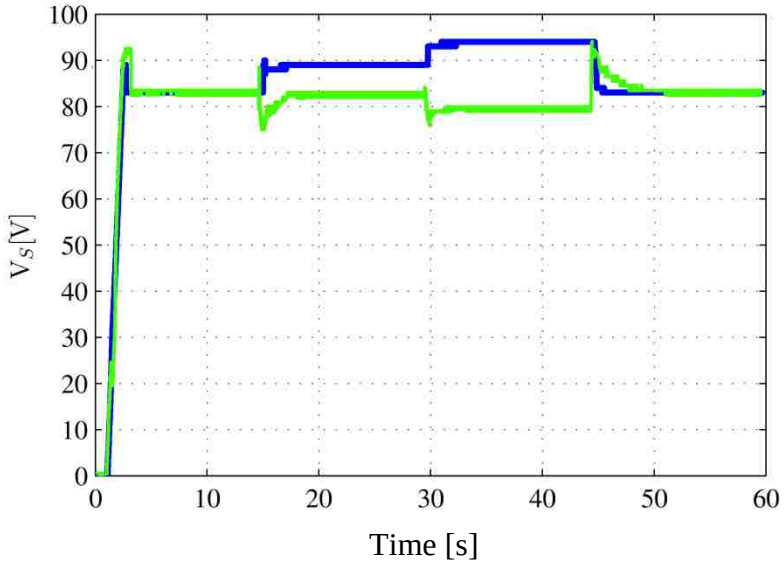

Figure 4.14. Comparison of stator voltage magnitude

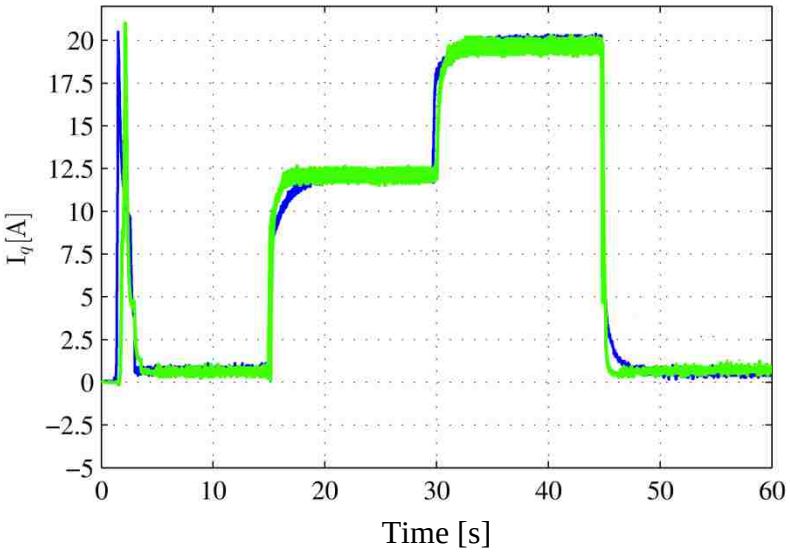

Figure 4.15. Comparison of stator current q component

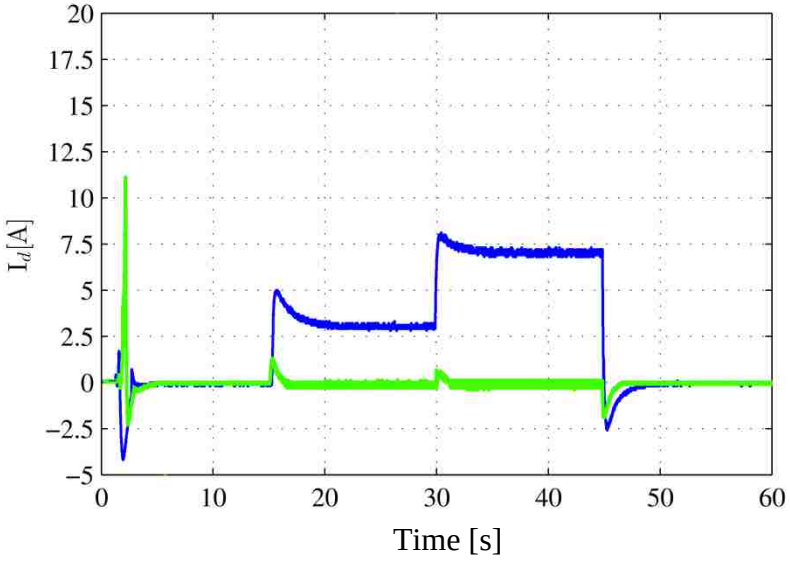

Figure 4.16. Comparison of stator current d component

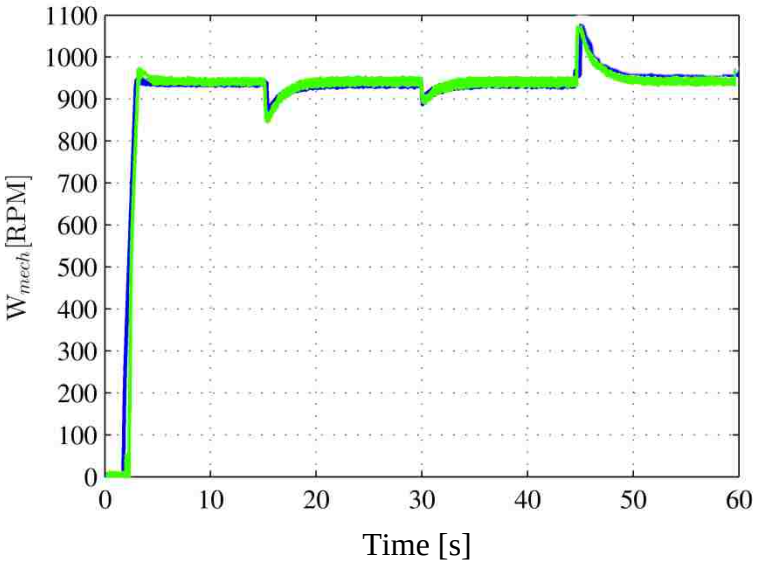

Figure 4.17. Comparison of rotor mechanical speed

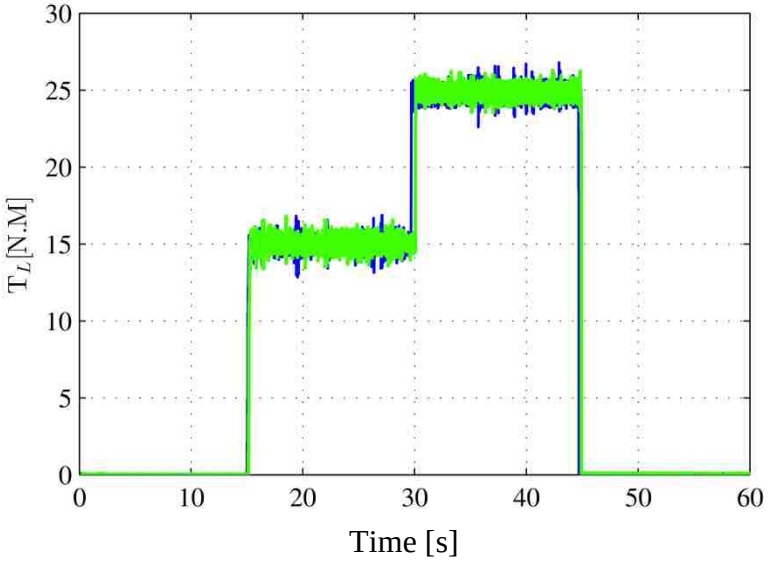

Figure 4.18. Comparison of applied load torque

4.3. ISSUES ENCOUNTERED DURING THE IMPLEMENTATION

When working with a relatively new technology such as automated generation for embedded targets some problematic issues are to be expected. Here, it is important to distinguish issues and the problems they cause from one another.

The most important issue is the reliability of the generated cod, i.e. that the code actually has the anticipated functionality. This has never been a problem through this project; the generated code has always functioned correctly and there have never been any compilation errors. This is most likely due to the Target Language Complier (TLC) in RTW which generates the code for all the different processor family packages, of which Target for TI C2000 is one. Hence a lot of development effort has been spent on the TLC and it appears to be very mature technology.

4.3.1. Software Issue. What has been an issue in the project are which blocks that are supported by code generation and which are not. The main problem is that all Simulink blocks that support code generation are not gathered in one or several block sets. Of course all the blocks that supports code generation, but to design the model more blocks are need such as summing and delay blocks, these blocks are found in the standard Simulink libraries. One illustrative example is that the unit delay block is supported but the integer delay block is not, even though they are basically identical in functionality.

In the case that user wants to use a fixed point DSP, another problem can happen through project development. The problem is that some of the standard Simulink blocks that support code generation does not support fixed point numbers. When using these clocks the signal must first be converted to integer or floating point then passed on to the block and then after the block be converted back to fixed point, something that of course highly degrades the efficiency of the generated code for the fixed point digital signal processor families. However the major issues encountered has not been regarding whether or not blocks support code generation or not but rather which DSP settings that are supported in the code generation. A tangible example of this problem is how the two hardware interrupt were initialized in the model that was developed. The interrupt generated in the ADC module, see section, and was initialized by selecting the post interrupt at end of conversion option in the properties pane of the ADC block.

The interrupt generated by the ePWM module was initialized in completely different and not very intuitive way, as described in section 2.2. This inconsistency in which settings that are implemented in different modules is quite confusing and disturbing for the designer.

When working in a rapid prototyping approach it is desirable for the designer to have the possibility to alter parameter values in real time or at least to alter them without rebuilding the entire program. This feature is possible in Matlab when using Simulink external mode, see [19], which enable logging and parameter tuning. However, this feature is only available using the CAN communication protocol which is getting used for implementation in this project. Particular for this project, using the CAN communication, the user easily can change the commanded speed of PMSM at any time after code generation whiles the test running.

It is noteworthy to mention here that parameter tuning and external mode is not compatible with IQmath/DMC blocks even when using CAN communication. This means that when the gains in for example a PID controller is to be changed, the whole program has to be regenerated.

4.3.2. Debugging. The debugging process when working with automated code generation is as anticipated fairly different compared to code written in the usual way. In the standard design process most syntax errors are found during the compilation of the program and are corrected in an iterative process unit the code compiles with the design rules.

In Matlab the syntax errors are found before the code is compiled, as Matlab executes the build command it checks the Simulink model and controls whether design rules are obeyed before he code is generated. Instead of an error message from the compiler the designer gets an error message from Simulink and the build process is halted before the code generation starts. Therefore there are seldom compilation errors.

The second part of the debugging process concerns the code functionality. Here the automated code generation has both advantages and disadvantages. The main advantage is the fact the code is auto generated. Thus registers, counters and memory sections are initialized correctly and without human mistakes. Since these are the main sources of functionality errors this is clearly an advantage and saves a lot of time and

effort for the designer. However, the main disadvantage is also due to the fact that the code is auto generated. The code generation is not perfect and if the generated code has errors these are very hard to find, although it appears to happen very rarely.

The most common debugging that has to be done when using automated code generation is to located functionality errors in the algorithm implemented in Simulink. These errors should generally be found during simulations before code generation. However, if they remain after the simulations they can be hard to be found by user since it is quite complicated to use break points in Matlab.

5. CONCLUSIONS

The idea of sensorless stable V/f control method for permanent-magnet synchronous motor (PMSM) drives was taken from earlier works where the idea was developed for low power permanent synchronized machine. The stabilized loop behavior is pretty much similar to the damper winding functionality which is not used in this application. Then a new optimization method suggested for a sensorless stabilized of the V/f control by minimizing the d-axis current which is proportional to the reactive power in the machine to reduce the motor losses, and supplied input power. The proposed sensorless method only needs machine terminal signals and does not require any additional motor parameters measurements. Minimization of the d-axis current is accomplished through computed reactive power.

The purpose of this thesis was also to examine a rapid prototyping approach using a CACSD to develop and implement a new motor control algorithm on a Digital Signal Processor (DSP), but instead of programming the DSP in Assembly or C, the main control algorithm will be performed in the Matlab/Simulink environment which is developed by the MathWorks^{TM}. Therefore, The DSP program was implemented using embedded code toolbox and Simulik/ Matlab. Moreover, the CAN communication was used in this work to communicate with DSP for reading the motor parameters ad sending commanded signal for dc drive.

Finally, the new developed algorithm was implemented for a PMSG drive which is a custom made drive built by the student design team using a TMS320F28335 DSP from Texas Instrument and a Semikron SKS. The program was run and tested for a 15 kW PMSM machine which directly connected to a dc machine controlled by a DCS800 ABB drive.

BIBLIOGRAPHY

[1] P. C. Krause, O. Wasynczuk, and S. D. Sudhoff, "Analysis of Electric Machinery, " IEEE Press, Piscataway,NJ, 1996.

[2] P. a. R. Krishnan, "Modeling of permanent magnet motor drives," IEEE , vol. 35(4), pp. 537-541, 1988.

[3] B. K. Bose, Ed., "Power Electronics and Variable Frequency Drives, " IEEE Press, Piscataway, NJ, 1997, chap. 6.

[4] T.D. Batzel, K.Y. Lee, "Electric propulsion with the sensorless permanent magnet synchronous motor: model and approach," IEEE Transactions on Energy Conversion, volume 20, number 4, pages 818-825, December 2005.

[5] K. Tatematsu; D. Hamada, "Sensorless permanent magnet synchronous motor drive with reduced order observer," IEEE Applied Power Electronics Conference volume 1, pages 75-80, February 1998.

[6] A. Piippo, J. Salomaki, J. Luomi, "Signal Injection in Sensorless PMSM Drives Equipped With Inverter Output Filter," IEEE Transactions on Industry Applications, volume 44, number 5, pages 1614-620, September/October 2008.

[7] S. Bolognani, L. Tubiana, M. Zigliotto, "Extended Kalman filter tuning in sensorless PMSM drives," IEEE Transactions on Industry Applications, volume 39, number 6, pages 1741-1747, November/December 2003.

[8] V.C. Ilioudis and N.I. Margaris, "PMSM sensorless speed estimation based on sliding mode observers," IEEE Power Electronics Specialist Conference, pages 2838-2843, 2008.

[9] R. Raute, C. Caruana, "Operation of a Sensorless PMSM Drive without Additional Test Signal Injection," IET Conference on PEMD, pages 616-620, April 2008.

[10] R.S. Colby and D.W. Novotny, "An efficiency-optimizing permanent-magnet.

[11] P.D.C. Perera, F. Blaabjerg, J.K. Pedersen, P.Thogersen , "A sensorless, stable V/f control method for permanent-magnet synchronous motor drives," IEEE Transactions on Industry Applications, volume 39, number 3, pages 783-791. May/June 2003.

[12] Matlab Help file section Embedded IDEs and Embedded Targets>> Working with Texas instrument C2000 Processors>> Configuring Timing Parameters for CAN.

[13] "C2000 TMS320x28x DSP System Control and Interrupts – Reference Guide, " Literature Number: SPRU078G, Texas Instrument, Revised August 2012.

[14] "TMS320x28x Analog-to-Digital Converter (ADC) – Reference Guide, " Literature Number: SPRU060, Texas Instrument.

[15] " TMS320x28x, Enhanced Controller Area Network (EV) – Reference Guide, " Literature Number: SPRU074, Texas Instrument. Revised June 2007.

[16] Copperhill Media Corporation, "A Comprehensible Guide to Controller Area Network , " Wilfried Voss , 2nd Edition, 2006.

[17] Vector Informatik GmbH , "CAN db++ Manual, " Version 2.7.

[18] Vector Informatik GmbH , "CANoe Software User guide, " .

[19] " Target Support Package TC23", the MathWorks, March 2008.

VITA

Seyed Hesam Jafari was born in Tehran, Iran. He received his Bachelor of Science degree in Power Electrical Engineering from Shahid Beheshti University, Tehran, Iran in February 2011. He started his Master of Science program in Electrical Engineering at Missouri University of Science and Technology in August 2011 and received his Master of Science degree in Electrical Engineering from Missouri University of Science and Technology in December 2013. His research interest includes Electrical machines drives, embedded systems and control and application of power electronic converters.